Dott. Ing. Giulio Soro

Fractal based image and video processing

PhD. Thesis

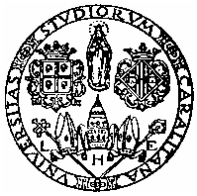

UNIVERSITÀ DEGLI STUDI DI CAGLIARI

FACOLTÀ DI INGEGNERIA

DIPARTIMENTO DI INGEGNERIA ELETTRICA ED ELETTRONICA

MULTIMEDIA AND COMMUNICATION LABS

Contents

Acknowledgment

To Prof. D.D. Giusto and Dr. M. Murroni without whom this work could not have been made, and to all of my family and friends who supported me along this part of life.

Foreword

This work is based on fractals. Since Barnsely demonstrated how to use these strange non-linear functions to encode images and Jaquin developed an automated fractal image compression algorithm, in just 14 years over 600 papers have appeared. This huge amount of study is due to the immense world of possibilities fractals give to researchers.

Fractals founded place in several fields of study, not only compression of images or video sequences or mathematics: economics, biology, geology, socials, and even politics.

The studies presented here, which derive from three years of research in this area, try to focus on the extremely promising property of implicit interpolation fractals gave us.

Since images, or more in general signals, are managed with the powerful concept of function instead of a collection of pixels, we can easily obtain interpolation between nodes of these functions.

This assumption leads to discover some amazing advantages that fractal encoding has compared to classical interpolation techniques.

Introduction

This work is divided in four chapters. The first chapter introduces the classical tecniques used to interpolate pictures, videos or signals in general. The problems of these interpolators are studied and confronted each other. The analisys of quality loss and errors introduced using the classical approach are the motivation that pushed us to work on the field of fractal to improve the interpolation quality.

Each of the following chapter focus on an aspect of fractal encoding and try to prove the improvement made using that tecnique.

The chapter two introduces the fractal theory and the use of fractals for encoding and decoding image. The decoding stage is extremely important because is at this stage that the actual zoom or interpolation is performed.

Since the image is decomposed at encoding time into a set of mathematical functions and correlations, at decoding time the interpolation is a mere multiplication by a scalar factor, i.e. a really simple step.

The simplicity of this step actually leads to a lot of quality loss. In fact using just *standard* fractal zoom leads to artifacts, blurring and a lot of other errors that masks the potentiality of the zoom.

To override these problems some we improved some existing tecniques and theories and our work was repaid by a great quality enhancement.

Third chapter analizes the key problem of this work, which is the interpolation using fractals of video sequences.

Since video sequences usually are huge amount of data, the analisys of video streams takes, even with fast machines, hours of working and are extremely complex.

To decrease the complexity while preserving quality we developed a framework for encode videos based on a combination of tecniques such wavelet decomposition, motion detection and

overlapping fractal encoding, prior to the interpolation phase, and then all the necessary operations needed to recombine the stream(s) during the final zoom.

The last chapter introduces our recent study about metrics and a new way to use a non-standard metric, known as EMD, to increase the quality of fractal encoding of color images.

Further study will be made on this last tecnique to test the validity of such interesting metric on the video fractal encoding.

Chapter I

I.1 Zooming tecniques

Currently, oversampling is often needed in several fields. In aerial or satellite imaging zoom is used in order to facilitate the image interpretation, or just to obtain a more comfortable visualization environment,

Available software realizes zooms using often some classical interpolators, which we briefly describe here.

These interpolators are particular oversamplers. An interpolator (or interpolation function) is a function which is equal to another function for some given points (interpolation nodes) [1]. That is the main differences between fractal oversamplers, described in the following sections, which do not necessarily keep the original luminance values. Each interpolator used in this work is a polynomial function.

The simplest oversampling is the Nearest-Neighbor Interpolation (N.N.I.). It consists in duplicating the original pixel's values. For example when zooming by a factor two, each original pixel is duplicated four times. So the degree of the polynomial function of interpolation is zero.

In practice the most frequently used oversampling is the Linear Interpolation (L.I.). This interpolator is based on a local hypothesis of luminance signal continuity and cylates by averaging [1] a value at a subpixel position.

The last interpolator we used as a reference is a modified version of the cubic one, the Cubic Convolution Interpolation (C.C.I) [3].

Nearest neighbor, linear and cubic convolution interpolators, which are approximation of the firs, second and third orders respectively, are based on local continuity hypothesis of the luminance signal and use a set of pixels located in a neighborhood (of resp. 1,4 and 16 pixels) around the position to be interpolated.

I.2 Slow motion tecniques

Among all possible interactive applications, widely used in classic analogic video reproduction, slow motion replay is one of the most expected to be extended to the digital formats.

Slow motion is a commercial feature of home video players, but also, a special effect used in the video production field. Its aim is usually to represent a slower replica of a fast sequence, making possible for the user to observe all the details of the scene which at regular speed could be lost.

In an analog framework, given a video sequence with a fixed frame rate f , the slow motion effect is obtained reducing the frame rate to $f' < f$, so that a frame remains visible for a time proportional to slow motion factor. This kind of slow motion, which does not involve any special technique, is usually the method that analog video players, like VCR equipment for example, use.

At present commercial digital video players allow users to browse a video sequence frame by frame or by chapter selection with prefixed indexes. Slow motion replay is classically achieved by reducing the frame rate display, just like analog slow motion, or keeping the frame rate constant and inserting within the sequence additional intermediate frames.

In a digital environment those frame can be generated by means of linear or cubic interpolation or simply repeating copies of frames along the time.

Interpolation along frames derives from classical interpolation of pixels within an image, and can be considered as oversampler. An interpolation (or an interpolating function) is a function which is equal to another function in some particular points called interpolation nodes.

The simplest oversampling function is the Nearest Neighbour Interpolator (N.N.I). It consists in duplicating the original pixels' values. For example when zooming an image by a factor of 2 (zooming factor = 2X) each original pixel is duplicated four times.

The N.N.I. is the base for digital frame replica slow motion. Every single pixel is duplicated along the time axis, of a factor equal to the desired slow motion factor.

One of the most frequently used interpolator in practice is the Linear Interpolator (L.I.). This interpolator is based on a local hypothesis of luminance signal continuity and calculates, by averaging, [2] a value at subpixel position. Another important interpolator, which we used as a reference, is the Cubic Convolution Interpolation (C.C.I.)[3].

All of these interpolations, N.N.I, L.I. and C.C.I., are approximation of the first, second and third orders respectively and are based on the concept of continuity of luminance signal of the pixels located on the neighbourhood around the position to be interpolated.

Concerning the video domain, the concept of L.I. and C.C.I. can easily be extended considering the values of pixel at the same position in adjacent frames as interpolating nodes.

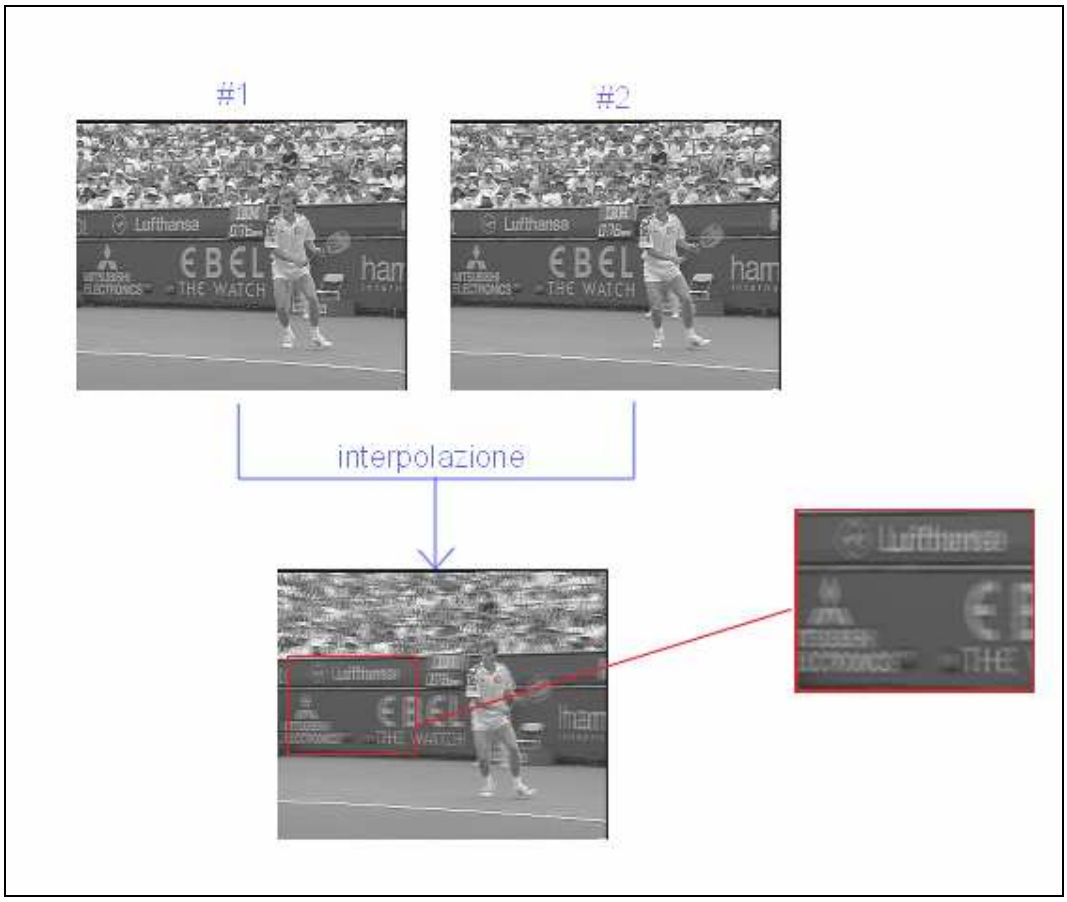

Fig. 1: Fading effect on interpolation

A major drawbacks of these approaches are that interpolation for slow motion replay yields to a "fading" effect between frames, whereas frame replication creates a "jerky" distortion, both resulting in low motion quality for the human visual system [26]. Similar issues arise in image plane if pixel replication or interpolation is used to perform spatial zoom.

These factors decrease the visual quality of the slowed sequence and, especially the *jerkiness* is considered by the Human Vision System (HVS) as an annoying distortion even for minor slow motion factors.

Both the terms *jerkiness* and *fading* will be completely addressed later on this work when we will introduce the quality metrics deployed by I.T.U [23] for the video quality assessment.

There are different kinds of interpolation that can be used for this purpose. In literature we found examples of classical interpolators as linear, cubic functions or more sophisticated tecniques such as splines or motion vector interpolation and motion compensation.

Some of those are used in this work as reference for quality measures, and could be found in the quality assessment chapter.

An intuitive definition of jerkiness is given as the discontinuity along the temporal axis of objects or group of pixels that move along the scene.

The Human Vision System (HVS) is particularly sensible to this kind of effects. This means that the quality of a slowed sequence is deeply degraded if the overall jerkiness is not kept under control.

A simply measure of jerkiness can be obtained considering the average square error between consecutive frames F_k e F_{k-1} :

$$S_{k,k-1} = \frac{\sum_{i=0}^{N-1}\sum_{j=0}^{M-1}\left(F_{k,i,j} - F_{k-1,i,j}\right)^2}{M \cdot N} \qquad \text{for } k = 1,\ldots,n$$

Where *M* and *N* are the width and height of frames and *S* is the jerkiness value between the couple of frames. This value is computer on the entire sequence. The graph below considers the value of jerkiness along 64 frames of *carphone* test sequence.

The graph shows the inner jerkiness of the original sequence, i.e. the *difference*, between adjacent frames. The aim of slow motion tecniques is to reduce the speed of the sequence without increasing the natural jerkiness of the video.

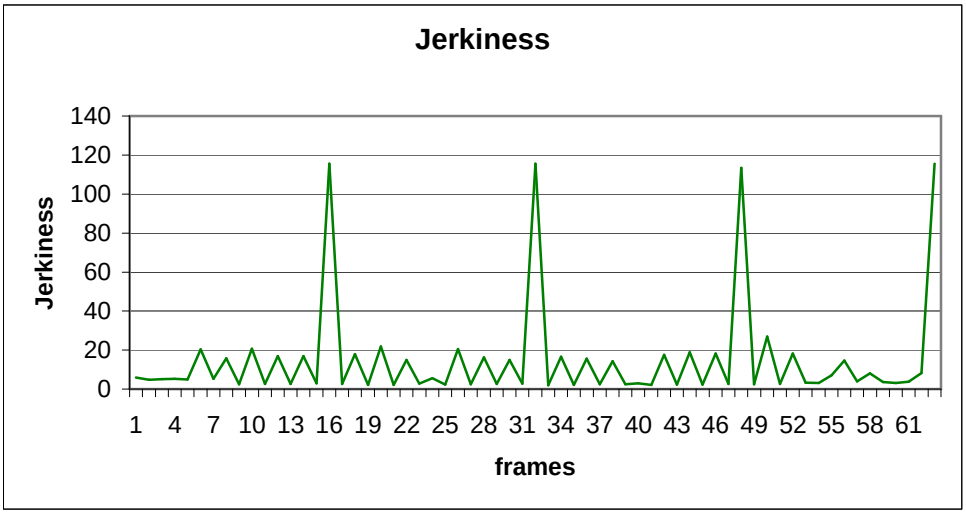

Fig. 2 Jerkiness values (RMS values) between frames of Carphone

Several works were published in the past on this topic. One of most interesting algorithm, based on motion estimation techniques, was developed at the B.B.C. labs by G.A. Thomas[4] and H.Y.K. Lau [5]: the frame was divided into partially overlapped blocks.

By means of Fourier analysis, a phase correlation was performed between corresponding blocks belonging to adjacent frames. Moving vectors were identified and interpolated to generate missing frames.

The main weakness of this technique is the inability to deal with the case of motion detection failure. This could occur due to the presence of high speed movement in the scene, so that the motion estimation algorithm was unable to find a good approximation of the movement for each block of the scene. Therefore, in presence of high speed movement in the sequence the effectiveness of the latter method decreases.

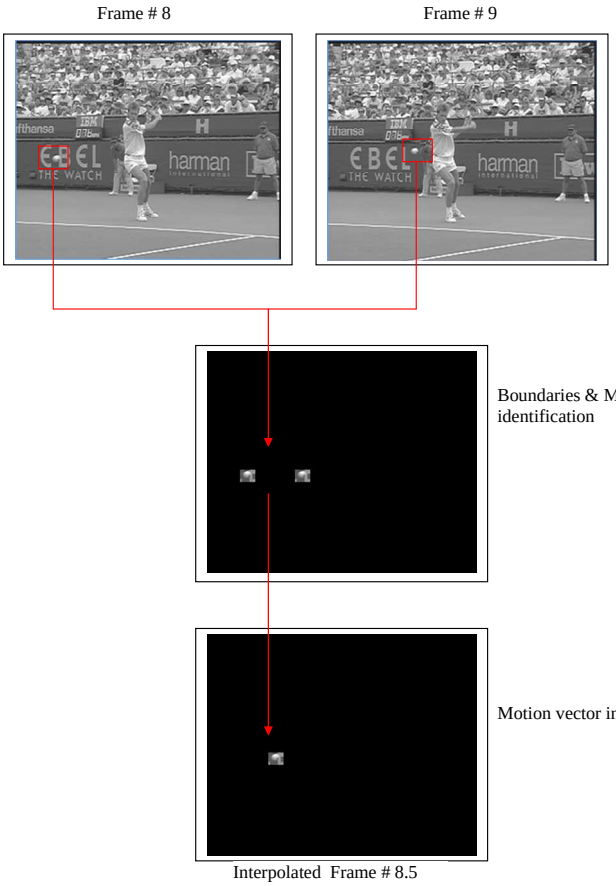

Fig. 3: Example of motion vector interpolation. After defining the motion vectors between blocks of different frames, an interpolation function is applied to find intermediate positions.

Fig. 4: Errors due to wrong interpolation. Sometime, especially on high ratio video sequences, motion vector leads to wrong positioning. This must be taken in consideration and a motion compensation algorithm for interpolated vectors should be adopted.

Other interpolation techniques were developed inside the framework of MPEG coding system. Some video coders in fact, drop frames from original video when the stream is coded with very low bitrates. To avoid enormous quality loss some techniques called Motion Compensated Interpolation (MCI) [6][7][8] were developed.

They try to exploit motion-compensated algorithms and obtain an interpolation of missing frames. These methods require no additional bandwidth and are usually integrated in MPEG or H.263 decoders.

In [9] the motion field already present in the encoded video is exploited to reduce redundant motion estimation usually needed as an extra computation by interpolators.

Comparisons between these methods will be shown later.

Chapter II

Fractals

II.1 Introduction

The name *fractal* was invented by Mandelbrot [10] and derives from the latin word *fractus*, which means broken in pieces.

In fact one of the most intuitive properties of this kind of objects is that can be thought as a lot of similar parts that make the whole object. Also the name refers to the important mathematical quality of this kind of *functions*: the dimension of fractals is not an integer value as the classical topological dimension. Actually the dimension of a fractal should not be computed using original Euclidian dimension D_T but introducing a new concept of dimension called Hausdroff-Besicovitch dimension [11].

Usually we think about fractals as complicated images and forms, perceiving them as static objects. Besides the fact that usually fractal images are *actually* complicated images, this point of view can hide the focal points of generations and evolution of fractal object, i.e. the *dynamic* properties of fractals.

There are some different definitions of how an object can be considered a fractal or not.

These include the properties of self-similarity, fine resolution, dense objects and so on.

Among these, the one that mostly can describe the mathematical properties of fractal can be the one that define a fractal by its dimension, based on the Hausdroff-Besicovitch definition.

In fact the mathematical definition of fractal that Mandelbrot introduces is of an object which its Hausdroff-Besicovitch dimension D_F is (not strictly) greater than its Euclidian dimension:

$$D_F \geq D_T$$

Instead, the most *intuitive* definition of fractal is of a figure, or better an object, composed by a motif that repeats itself scaled or rotated at every resolution. This leads to a fractal as a *dense* and *fine* function, as mentioned above.

Given that, a zoomed part of a fractal will always contain infinite points at every grade of zooming factor. More, the position of this point is imposed by the motif pattern defined by the equation that creates the *fractal*. This last point gives us the intuition on how important is the *evolution* and the *dynamic properties* of a fractal.

The theory was defined mathematically by Mandelbrot in the XX century but the first step and discoveries of these strange functions go back in time.

Classical *pre-fractals* (as they are called since the definition of fractal was not yet given) are the ones invented by Cantor, Sierpinski and many others.

But the inner properties and use of fractals could be achieved only when the computational power of computer appears.

Joined with the *chaos theory*, fractals could be then used to create models for many natural events like clouds geometry, metereological events (Lorentz [12]), terrain and natural object's geometry, lighting distributions and so on.

In fact fractal geometry creates approximations of natural objects closer than approximations created using the classical Euclidian geometry.

This will lead, as we will see later, to a better *realism* of zoomed images with fractals functions compared to classical interpolators based on the Euclidian geometry.

Fractals also appeared to be a good mathematical framework for image and, as we will explain in this work, video compression and processing exploiting the fact that those images have a lot of inner redundancy.

A lot of works have been done to create image compressors like the famous JPEG and JPEG2K as for video (MPEG1, MPEG2, MPEG4 and others..).

Fractal image compression born in the 80s of the XX century, mostly by studies leaded by Barnsley [13], Jaquin [14] and Fisher[15].

As we will see on the following part of this work, a lot of properties besides compression can be obtained using fractals for image and video coding instead of common techniques as the ones mentioned above.

II.2 Fractal coding

Since fractals can be intended as collection of similar parts defined by a common motif (or *pattern*) derived by some mathematical functions, the fractal encoding can be thought as the search for this motif inside a natural image.

For being a fractal, an object F must satisfy some properties:

1. *Self-similarity: F must be composed by copies of itself at different scale rate*
2. *Fine structure: F must have details at every resolution*
3. *Recursivity: the function Z from which F derives has to be recursively defined:* $F = \{Z \mid Z = f(f(f(...)))\}$
4. *Dimension:* $D_F > D_T$

A classical example of how to create a fractal is by means of a simply algorithm that copies and scales an initial image given as input. This algorithm, known as the Barnsley copy machine (or the Multiple Reduction Copy Machine MRCM), takes an initial image μ_0 and creates as output three copies of it displaced on the vertexes of an equilateral triangle and reduced by a factor of $1/3$.

After this step the output is taken as the new input for the algorithm and the process starts again.

If we call this function τ_Δ, and $\tau_\Delta(\mu_0)$ the result we obtain, the first step the output of the algorithm leads to the image shown in Fig. 5.

μ_0 τ_Δ $\tau_\Delta(\mu_0)$

Fig. 5: Application of algorithm τ_Δ to the initial image μ_0 using the MRCM

If the process is taken again indefinitely, the output image starts to converge to a precise image, totally different from the starting one. We call this ending image the *attractor* of the function τ_Δ. Mathematically we say that the attractor $\mu_a = \lim_{k\to\infty} \tau_\Delta^k(\mu_0)$.

The first five steps of the transformation τ_Δ are shown in Fig. 6.

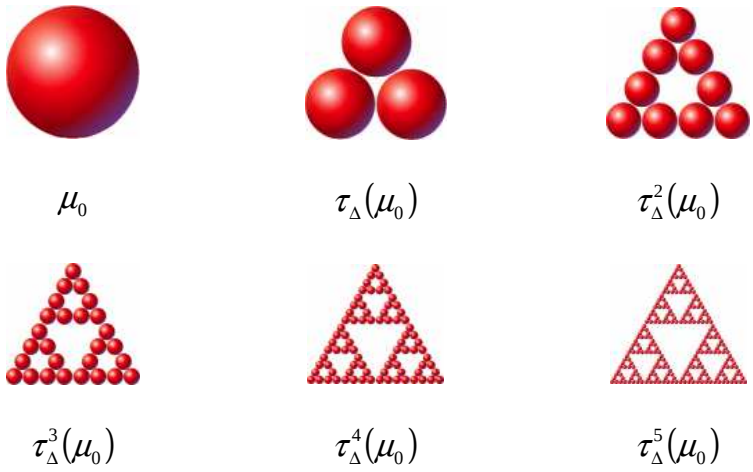

μ_0 $\tau_\Delta(\mu_0)$ $\tau_\Delta^2(\mu_0)$

$\tau_\Delta^3(\mu_0)$ $\tau_\Delta^4(\mu_0)$ $\tau_\Delta^5(\mu_0)$

Fig. 6: five iterations of τ_Δ for the starting image μ_0

As we see, the attractor for this function is the Sierpinski's triangle, and is completely defined by the rules contained in the function τ_Δ. A focal point of this example is how the final image (the Sierpinski's triangle) is completely independent from the initial image (the ball), as demonstrated in Fig. 7.

This means that instead of storing every single point, at every resolution, of the Sierpinski's Triangle, only τ_Δ can be stored and the triangle can be re-obtained from any other image just

applying the τ_Δ to it. This last sentence gives some hints about the relation that can exist with fractals and compression.

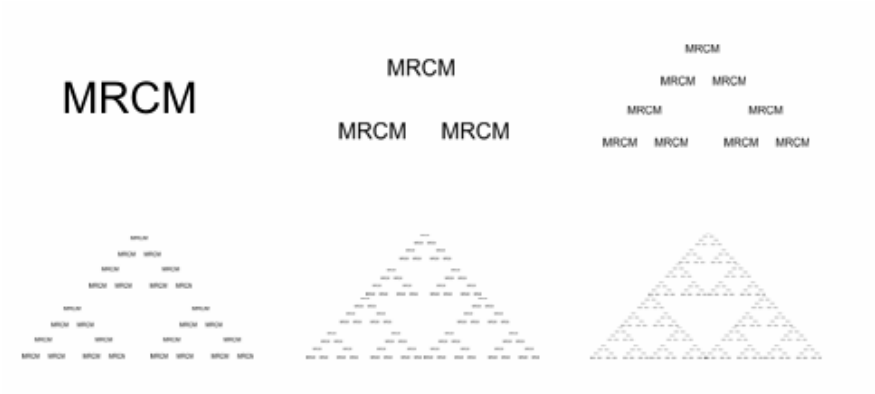

Fig. 7: six iterations of MRCM starting from the word "mrcm"

If we inspect τ_Δ we can observe that it is composed by simpler functions, like scaling I_s ($\frac{1}{3}$ of the original) and translations I_t (on the vertex of a triangle) so that:

$$\tau_\Delta = I_s \circ I_t$$

Changing these functions, that means altering τ_Δ, leads to change the attractor.

So we can say that the attractor is completely defined as we define the functions that identify τ_Δ. The issue now at this point is to define the set of functions that can be used to create a general τ_Δ.

The fractal theory states that any transformation can be used to compose a τ_Δ but it has to be a contractive function.

Being contractive is the only limitation we have: it is necessary as the iterations of the τ_Δ converge. If the functions chosen to build up the τ_Δ are not contractive the iterations can diverge and will not lead to a stable attractor.

Mathematically a transformation τ is said to be contractive if, given a distance metric d and $s \in \Re : 0 \le s \le 1$, we prove that:

$$d(\tau(a), \tau(b)) \le s \cdot d(a,b); \quad \forall a,b \in C$$

With *C* being the space of points we consider.

Back to the example shown above, the contractivity *s* is assured by the scaling factor $1/3$ of I_s (can be proved that the contractivity of a translation I_t is $s = 1$).

The number of functions that respect the property defined is huge, so for our purposes we can limit our functions to a class, called *affine transforms*, that is enough for create a sufficient sets of attractors.

An affine transform is a bijective transform that maps a point $P(x_1, x_2, ..., x_n) \in \Re_n$ onto a point $P'(y_1, y_2, ..., y_n) \in \Re_n$ so that $\overline{Y} = A\overline{X} + B$ with $A, B \in \Re_n$ and $\det(A) \neq 0$.

Usually in literature the class of affine functions used to build up fractals, for image compression purposes are isometries, eight of which are shown as example in Fig. 8 and described in Table 1.

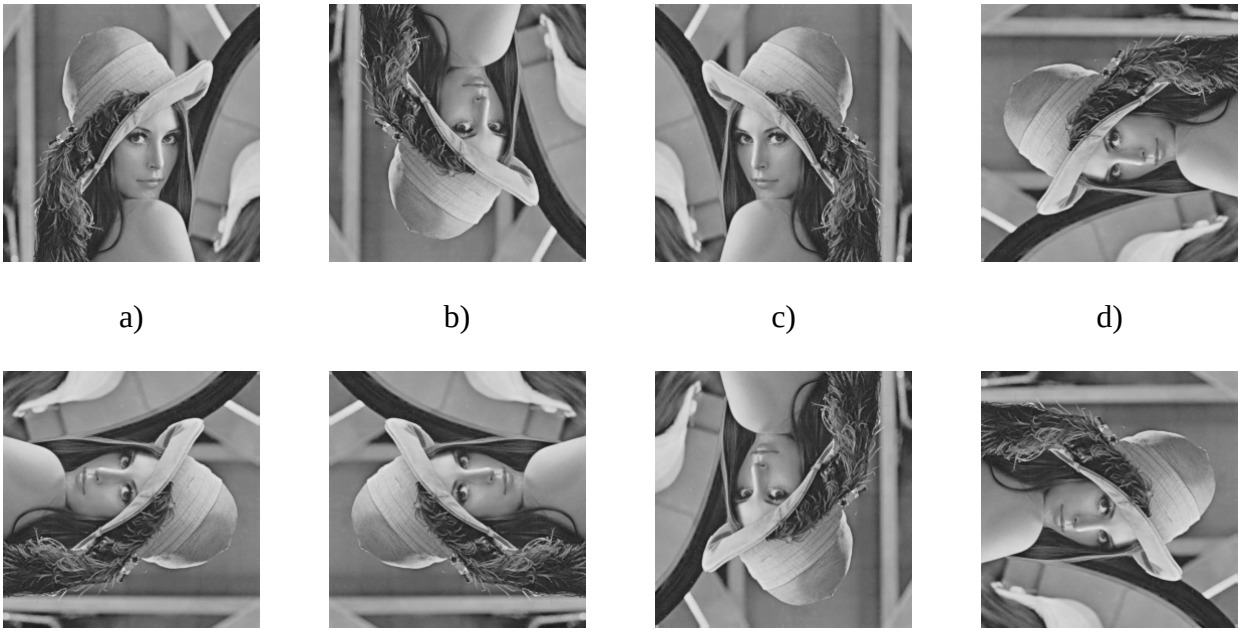

a) b) c) d)

e) f) g) h)

Fig. 8: Isometries used for fractal compression applied to test image *Lena*

Identity (a)	$\tau_1(\mu_{i,j}) = \mu_{i,j}$
Horizontal reflection (b)	$\tau_2(\mu_{i,j}) = \mu_{i,n-j}$
Vertical reflection (c)	$\tau_3(\mu_{i,j}) = \mu_{n-i,j}$
First diagonal reflection (d)	$\tau_4(\mu_{i,j}) = \mu_{j,i}$
Second diagonal reflection (e)	$\tau_5(\mu_{i,j}) = \mu_{n-j,n-i}$
90° rotation (f)	$\tau_6(\mu_{i,j}) = \mu_{n-j,i}$
180° rotation (g)	$\tau_7(\mu_{i,j}) = \mu_{n-i,n-j}$
270° rotation (h)	$\tau_8(\mu_{i,j}) = \mu_{j,n-i}$

Table 1: description of isometries shown in Fig. 8

In $\Re^2$, the equation can be expressed as

$$\begin{bmatrix} x_{new} \\ y_{new} \end{bmatrix} = \begin{bmatrix} a & b \\ c & d \end{bmatrix} \begin{bmatrix} x \\ y \end{bmatrix} + \begin{bmatrix} e \\ f \end{bmatrix} = A\bar{x} + B$$

Where A is a scaling and rotation matrix whereas B is a translation vector.

Being a point $P = (x, y)$ we can define a scaling operation S, yielding a new point $P' = (x', y')$. In formulas:

$$\begin{cases} x' = s \cdot x \\ y' = s \cdot y \end{cases}$$

With $s > 0$. A scale reduction occurs if $s < 1$, while an enlargement will be produced if $s > 1$; using the matrix notation we have that a scaling will be made using:

$$A = \begin{pmatrix} s & 0 \\ 0 & s \end{pmatrix}$$

Next, a rotation R is applied to $P' = (x', y')$ yielding $P'' = (x'', y'')$

$$\begin{cases} x'' = \cos\theta \cdot x' - \sin\theta \cdot y' \\ y'' = \sin\theta \cdot x' + \cos\theta \cdot y' \end{cases}$$

The rotation is counter-clockwise, rotating the object of an angle equals to teta. The matrix notation is:

$$A = \begin{pmatrix} \cos\theta & -\sin\theta \\ \sin\theta & \cos\theta \end{pmatrix}$$

Finally a translation T of P'' can be obtained using a displacement (T_x, T_y):

$$\begin{cases} x''' = x'' + T_x \\ y''' = y'' + T_y \end{cases}$$

That is a translation vector:

$$B = \begin{pmatrix} T_x \\ T_{y\partial} \end{pmatrix}$$

II.3 Iterated Function Systems for Image Encoding

The technique that leads fractal theory to image compression for general purposes derives from the concept of Iterated Function Systems (I.F.S.) [13]. As mentioned before, IFS are fractals generated by means of affine transforms.

To code an image using fractal, the IFS method is posed backward.

Given the image μ that we want to code, we state that this image μ is the attractor of some transformation τ generated by combinations of elementary functions taken by the affine set described above (i.e.: isometries, scaling factors…).

The issue is to find these functions so that applied to any arbitrary image μ_0 for $k \to \infty$ iterations $\tau^k(\mu_0)$ converge to the given initial image μ. This is called the *inverse problem.*

The theory, proven by Barnsley, states that if we assure that the functions used are contractive the solution of the problem exists (collage theorem), and the final image is actually composed by tiny copies of the initial image.

The Barnsley method of encoding an image is not actually applicable. We can instead use a sub-part of the method, discovered by Jaquin, using what is called *Partitioned Iterated Function Systems.*

Instead of considering the whole image itself, we consider subparts of it and look for similarities inside the image. The starting image μ is partitioned into subsets (usually squared blocks) and a matching process is started to find which subsets can be approximated by other subsets transformed by the affine set chosen.

After the matching process, only the transformations are stored, achieving a compression factor for image storing. An example of similarities present in a test image is given in Fig. 9.

Fig. 9: some similarities in test image *Lena*

The set of transform stored is used at the decoding stage. These transforms are applied to an initial image μ_0, usually blank, and iterated for n steps depending, as we will see, on PSNR ratio.

This encoding method is a *lossy* technique. In fact the matching process is not perfect and also iterations will not go forever.

Basically, fractal coding of an image consists in building a code τ (i.e.: a particular transformation) such that, if μ is the original image, then $\mu \approx \tau(\mu)$, that is, μ is approximately self-transforming under τ.

The Collage Theorem states that if τ is a contractive transformation, μ is approximately the attractor of τ, that is $\mu \approx \lim_{k\to\infty} \tau^k(\mu_0)$ for the some initial image μ_0.

The code τ is built on a partition of the original image. Each block R_i of this partition is called *range block* and is coded independently of the others by a matching (local code τ_i) with another block D_i of the image, called *domain block*. If R and D are the range and domain block's sizes (in case of squared blocks) respectively, then $D = p \cdot R$ with $p > 1$ scaled factor used for the local self-similarity search.

Classical τ_i transforms are isometries (i.e.: rotations flip, etc.) and massive transform (i.e., contrast scaling and grey shifting).

If L is the number of range blocks, the fractal code of the initial image is then

$$\tau\left(\mu_{orig}\right)=\bigcup_{i=1}^{L}\tau_i$$

Where $\tau_i : D_i \to R_i$ and $\tau_i = M_i \circ I_i \circ r_{i,p}$ with $M_i\left(x\right)=a_i \cdot x+b_i$ an affine operator with a scale a_i and a shift b_i on the luminance pixel, I_i a transformation selected from eight discrete isometries and $r_{i,p}$ a reduction by a factor p using an averaging.

In other words, the task of the fractal encoder is to find for each range block a larger domain block such that, after an opportune transformation, this constitutes a good approximation of the present range block. An example is shown in Fig. 10

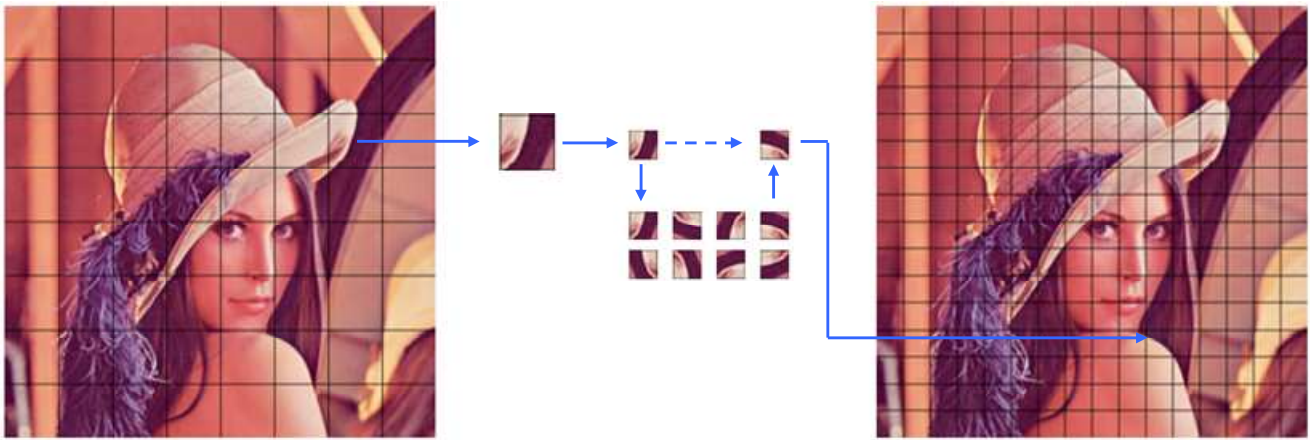

Fig. 10: Example of domain to range block mapping for *Lena*

The fractal code for the original image is a collection of so extracted local codes. This approach implemented by Jaquin gives a representation of the image as composed by copies of parts of the image itself. The classical fractal decoding stage consists in an iterated process starting from an arbitrary initial image μ_0. In fact, if τ is a contractive transformation the τ's attractor $\tau^{\infty}(\mu_0)$ gives an approximation of the original image μ independently from the initial image.

II.4 Decoding stage

At decoding, starting from any μ_0 initial image, the fractal code is reversely applied: μ_0 is partitioned in the same number of range and domain blocks of the encoded image.

For every μ_{0_i} range block, the corresponding τ_i coded for the i-esim range block of the original image is applied.

This means that the right domain block of μ_0 is taken, the right isometry in applied and then mapped to the range block.

This process is made for every range block of μ_0. The output $\tau^1(\mu_0)$, made of the collage of the entire range block transformed, is then used back as the input of the algorithm and the process starts again.

After n iterations the image $\tau^n(\mu_0)$ converges to a close representation of the original image.

Usually the n iterations are chosen using PSNR threshold. When the PSNR difference between $\tau^{n-1}(\mu_0)$ and $\tau^n(\mu_0)$ is less than 0.1 dB iterations are stopped.

An example of different quality obtained for different iterations of the algorithm is given in Fig. 11 while PSNR difference is given in Fig. 12.

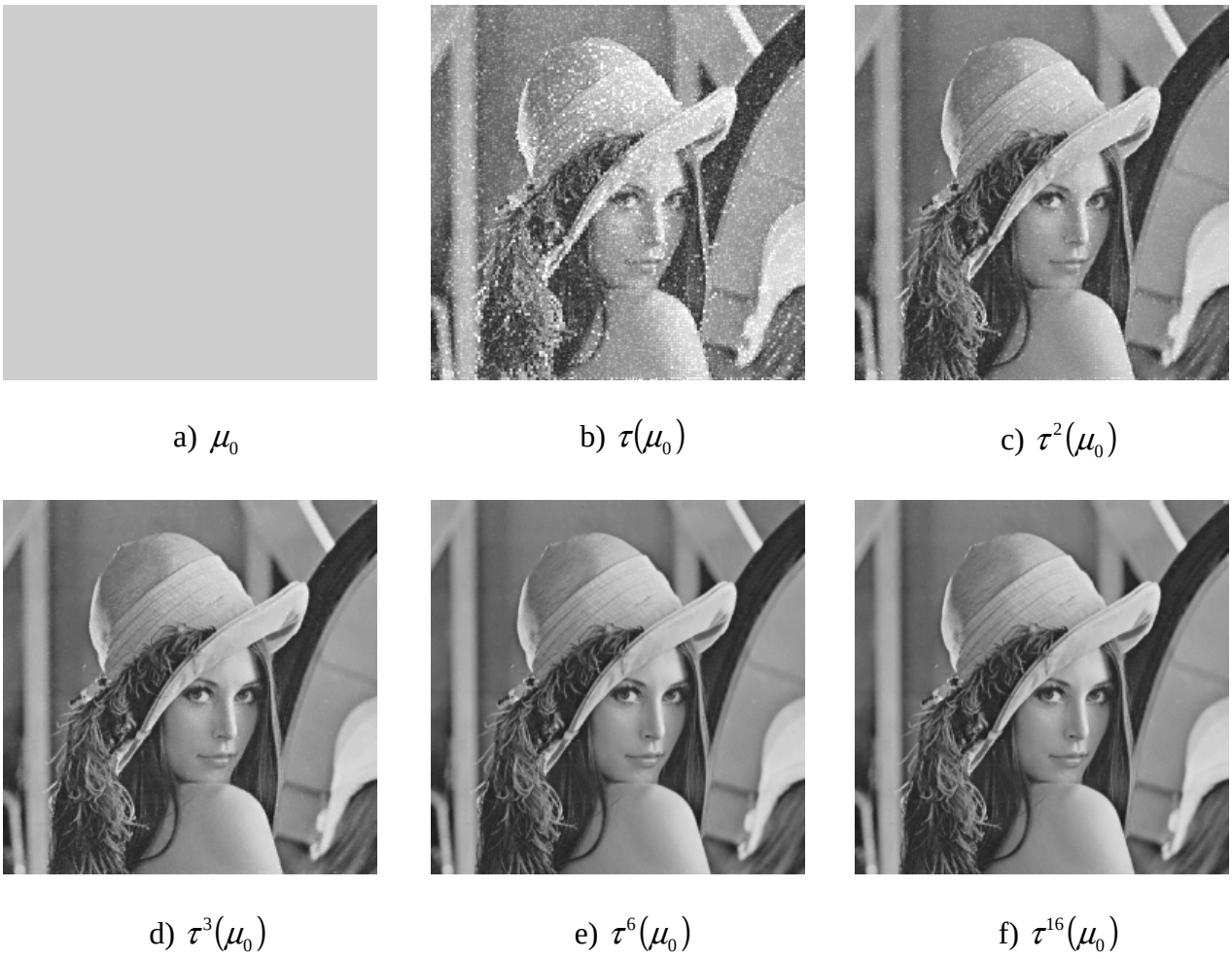

a) μ_0 b) $\tau(\mu_0)$ c) $\tau^2(\mu_0)$

d) $\tau^3(\mu_0)$ e) $\tau^6(\mu_0)$ f) $\tau^{16}(\mu_0)$

Fig. 11: example of different iterations for *Lena*

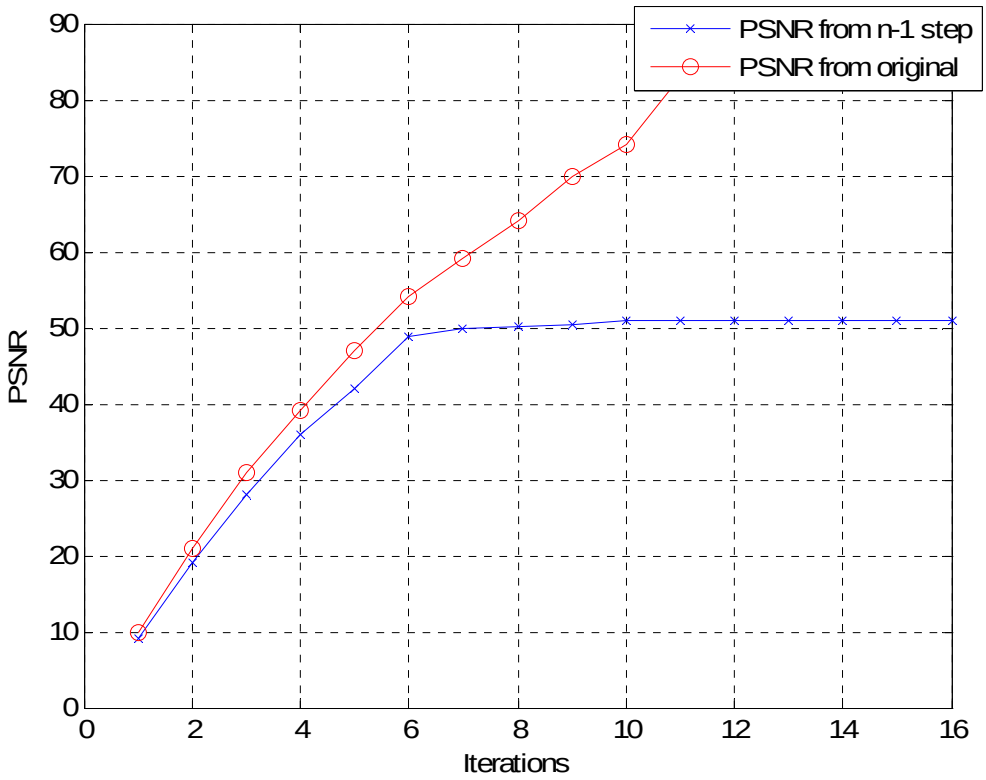

Fig. 12: PSNR values over iterations

II.5 Fractal zoom

One of the most important features of fractal encoding is hidden into its mathematical representation.

Since the image fractally coded can be thought as a mathematical function, given by the collection of τ of every block, i.e. $\tau\left(\mu_{orig}\right)=\bigcup_{i=1}^{L}\tau_i$, and these are isometries, we can obtain easily a larger scale of the original image.

In fact, if $\overline{Y}=A\overline{X}+B$ is a chosen isometry that maps the point $\overline{X}\in\Re^n$ to $\overline{Y}\in\Re^n$ we can obtain a zoom simply by a scalar multiplication so that

$$\overline{Y_{zoomed}}=s\cdot A\overline{X}+s\cdot B$$

With s being the zoom factor.

Pratically the fractal code extracted from the original image has itself everything necessary to obtain a zoomed replica of the image.

Usually this property is called implicit interpolation, because no explicit formulas are used to obtain interpolation between pixel, and all the information required is taken during encoding time.

To use this property of fractals with our technique, based on P.I.F.S. encoding, we decode the image using range blocks and domain blocks greater than the ones used on encoding stage.

More, the fractal code itself does not give any information about the range or domain block size used during the encoding, so we can apply the same fractal code to different sizes of blocks.

If for example we star encoding an image with range blocks of size $n\times n$ pixels but during the encoding we apply the extracted fractal code to range blocks of size $m\times m$, with $m>n$, we obtain a zoom factor of m/n.

Literature has proven that overall quality of images zoomed using fractal encoding is better compared to techniques like common interpolation techniques as linear, cubic or spline interpolation.

Usually quality of zoomed image is extremely difficult to evaluate, since standard metrics as PSNR are objective metrics, whereas the quality of a zoomed image is a perceived feature. An example is given in Fig. 13.

a) b) c)

Fig. 13: example of different zoom tecniques applied to a *Lena* subpart: a) Nearest Neighbour, b) linear interpolation, c) Fractal zoom

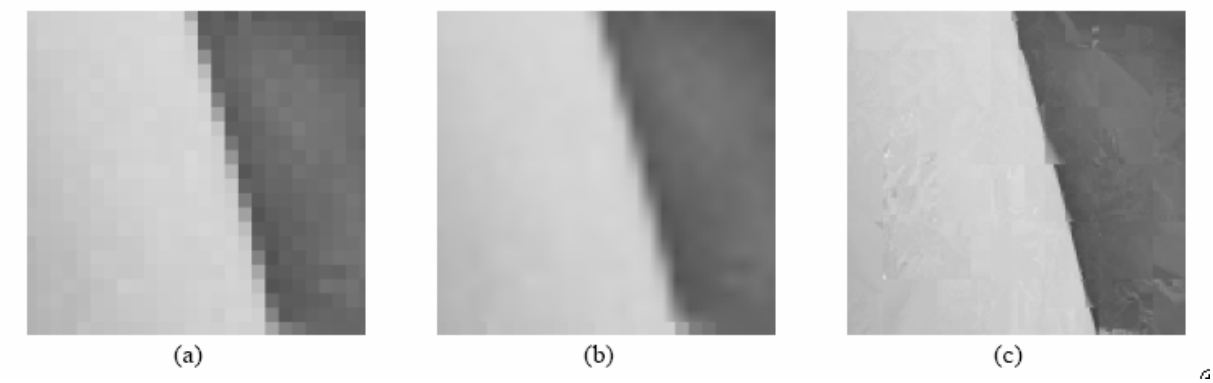

Fig. 14: a closed view of zoomed images: a) Nearest Neighbour, b) linear interpolation, c) Fractal zoom

II.6 State of the art for fractal zooming

The main problem of fractal zoom is that for big zooming factor, blockness distortion decreases the overall quality of the output image.

This is due to the fact that fractal encoding as described above involve a block partition exactly at the first stage of the process.

These artefacts are responsible of high frequencies on the decoded image that were not present in the original image.

A method that improves the quality of the fractal zoom was developed by Reusen [18] and Polidori [25].

Since the inner problem is partitioning into range blocks, the blockness effect can avoided just using an overlapped range block partitioning (O.R.B).

The original image is partitioned in four different ways so that range blocks of a partition overlap the other partitions' range blocks.

The classical method was intended by means of range blocks of size R and domain blocks of size $D = p \cdot R$. This means that a range block is distant R from another one. Given the original image μ to be encoded, we can identify four other partitions considering different parts of μ:

- $\mu|_1$ is the original μ;
- $\mu|_2$ is obtained taking off two strips of pixels $R/2$ wide at the left and at the right of μ;
- $\mu|_3$ is obtained taking off two strips of pixels $R/2$ wide at the top and at the bottom of μ;
- $\mu|_4$ Is obtained taking off four strips of pixels $R/2$ wide both at the left and at the right and at the top and at the bottom of μ.

Every $\mu|_i, i = 1,...,4$ is then again partitioned using blocks of size R.

This method assures us that every range block of the original partition is covered several times with the blocks of the other three partitions. An example of these four partitions is shown in Fig. 15.

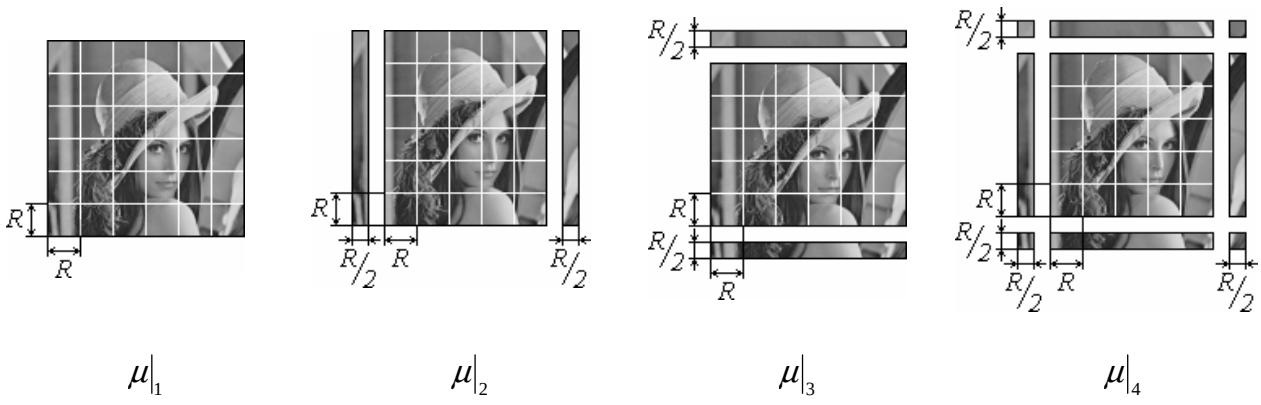

Fig. 15: different partitions for *Lena*

These four partitions are than coded independently. This leads to four different fractal codes $\tau|_1, \tau|_2$ $\tau|_3$ and $\tau|_4$ for one initial image μ so that the global fractal code is $\tau = \sum_{i=1}^{4} \tau|_i$ [1].

At decoding time every $\tau|_i$ will be used to obtain a target image $\tau|_i(\mu_i)$.

The four target images then are melted together to obtain the final image using a filtering operator Ψ_{OSO}. Usually this O.S.O. (Ordered Square Overlapping) operator is a classical median filter.

The decoding stage with O.S.O. filtering and zoom expansion is shown in Fig. 16 while the complete process is shown in Fig. 17.

[1] Here the operator $\sum$ is intended as a concatenation of fractal codes.

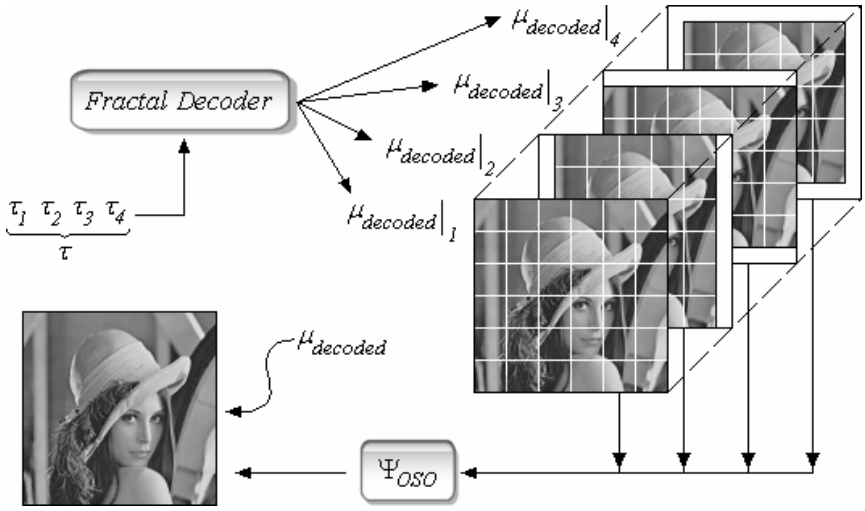

Fig. 16: O.S.O. decoding example for *Lena*

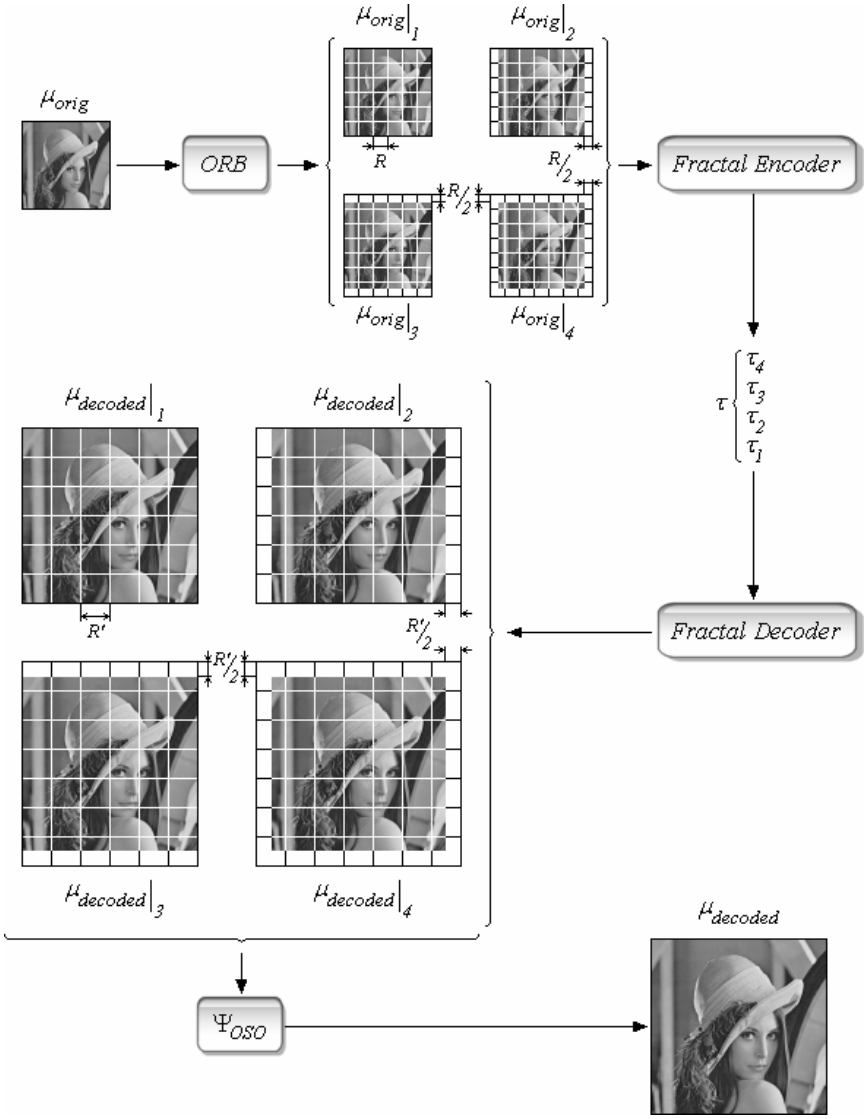

Fig. 17: fractal encoding/decoding with O.R.B. and O.S.O.

This technique improves greatly the quality of zoomed images with the fractal method.

The overall gain of quality using fractal theory for zooming is good. Usually the quality gap between classical interpolators as linear, bicubic or splines and fractal zoom increases in favour of the latter when high zoom factor are used.

The table below shows different PSNR values for zoom for different techniques and zoom factors.

Chapter III

Fractals and video sequences

III.1 Introduction

This chapter describes the work done to extend the classic theory of fractal encoding and fractal interpolation from the image field to the video sequence area.

The purpose of this research was intended to extend fractal interpolation to cover the problem of slow motion of video sequence.

The enormous amount of data in a sequence leads to problems like complexity reduction and algorithm optimizations. This chapter will introduce the wavelet transform of signals and how its use, joined with some other technique, gave us the possibility of overwhelming the issues described above.

Slow motion is a special effect used also in the television broadcasting production field. It is a filmmaking technique in which the action on screen is slower than normal. Already consolidated as a feature within analog TV production studios, today slow motion is likely to be extended to the Digital Video Broadcasting (DVB) technology. At present, slow motion is performed during the pre-production stage by means of fast-shuttered cameras able to capture the scene at a frame rate higher than the standard rate that is 25 Frame/sec for PAL/SECAM systems and 30 Frame/sec for NTSC systems. Slow motion is achieved by filming at a speed faster than the standard rate and then projecting the film at the standard speed. In this case an optical zoom is executed and the slow motion factor achievable is limited to shutter speed and fixed during the pre-production stage. In a

digital video production higher slow motion factors can be achieved by means of video post processing techniques aiming at enhancing the performance of the fast-shuttered cameras by inserting intermediate frames within the captured sequence. This process is normally referred as digital zoom. Intermediate frames can be a replica of the previous frame, or can be generated by means of interpolation. In the latter case, either linear or cubic spline functions can be used. Both frame replication and interpolation have some drawbacks: interpolation for slow motion replay bears to vanishing effects, as well as frame replication yields to jerky motion, both resulting in low perceived quality to human vision system. An original solution to these problems based on motion detection techniques was proposed at the BBC labs by G.A. Thomas [4] and H.Y.K. Lau [5] the frames were divided into partially overlapped blocks; by means of Fourier analysis, a phase correlation was performed between corresponding blocks belonging to adjacent frames. Moving vectors were identified and interpolated to generate missing frames. The main weakness of this technique was the inability to deal with the case of motion detection failure. This could occur due to the presence of high speed movement in the scene, so that the motion estimation algorithm was unable to find a good approximation of the movement for each block of the scene. Therefore, in presence of high speed movement within the sequence, the effectiveness of the method significantly decreased. In this work, we propose an alternative post processing scheme which combines the properties of expansion, given by fractal representation of a video sequence, with motion detection techniques and wavelet subband analysis to overcome the limitations of the state of the art solutions.

In literature, fractals on image applications were proposed to achieve data compression exploiting self-similarity inside natural images.

But the potentiality of fractals is not limited to compression. The properties of fractal coding allow expanding a multi-dimensional signal (e.g., image and video sequences) along its dimensions. One of the major weaknesses of the fractal representation of a signal is the high computational complexity of the encoding process. The computational load, and so the processing time, increases for signals of higher dimension (1D, 2D, 3D…).

This is due to the fact that the main idea of fractal encoding is to look for similarities of blocks using affine transforms, therefore a best match algorithm leads to a great time consuming process for multi-dimensional data sets. Several methods have been proposed in literature to speed up the fractal coding process [16]. A class of proposed solutions is based on wavelet subband analysis. Due to their orthogonal and localization properties, wavelets are well suited (and extensively adopted) for subband data analysis and processing.

The proposed algorithm exploits these features performing the fractal coding of each subband with particular attention to the frequency distribution of the coefficients. To further reduce the high computational cost of fractal encoding, active scene detection is used so as to perform fractal coding only in high information areas (moving areas). As suggested in [18], to improve overall visual quality overlapped block coding and post process filtering, extended to the three dimensional case, are used.

Results show that with the proposed approach the quality achieved is higher if compared to the state of the art techniques.

III.2 Fractal coding of video signals

The theory described in Chapter II for encoding an image by means of fractals, can be extended straightforward to video signals.

In fact, a video signals can be thought as a ordered collection of images, called now frames, that give information about changes along time.

There are different ways of how to encode video using fractals.

We can think of the frames as an independent stream of data and encode them independently.

So if a video sequence is composed by n frames:

$$S = \bigcup_{i=1}^{n} \mu_i \qquad \textit{Eq. 1}$$

We can obtain the encoded stream just searching for appropriate transformations τ_i on every single frame, so that the output video is:

$$S' = \bigcup_{i=1}^{n} \tau_i(\mu_0) \qquad \text{Eq. 2}$$

$$S' \xrightarrow[n\to\infty]{} S$$

Being μ_0 an initial arbitrary frame. Coding a video sequence in this way does not introduce anything new, besides is not capable of reduce the redundancy between frames which in a video sequence is extremely high (Fig. 18),. In fact most of the frames are correlated each other along time.

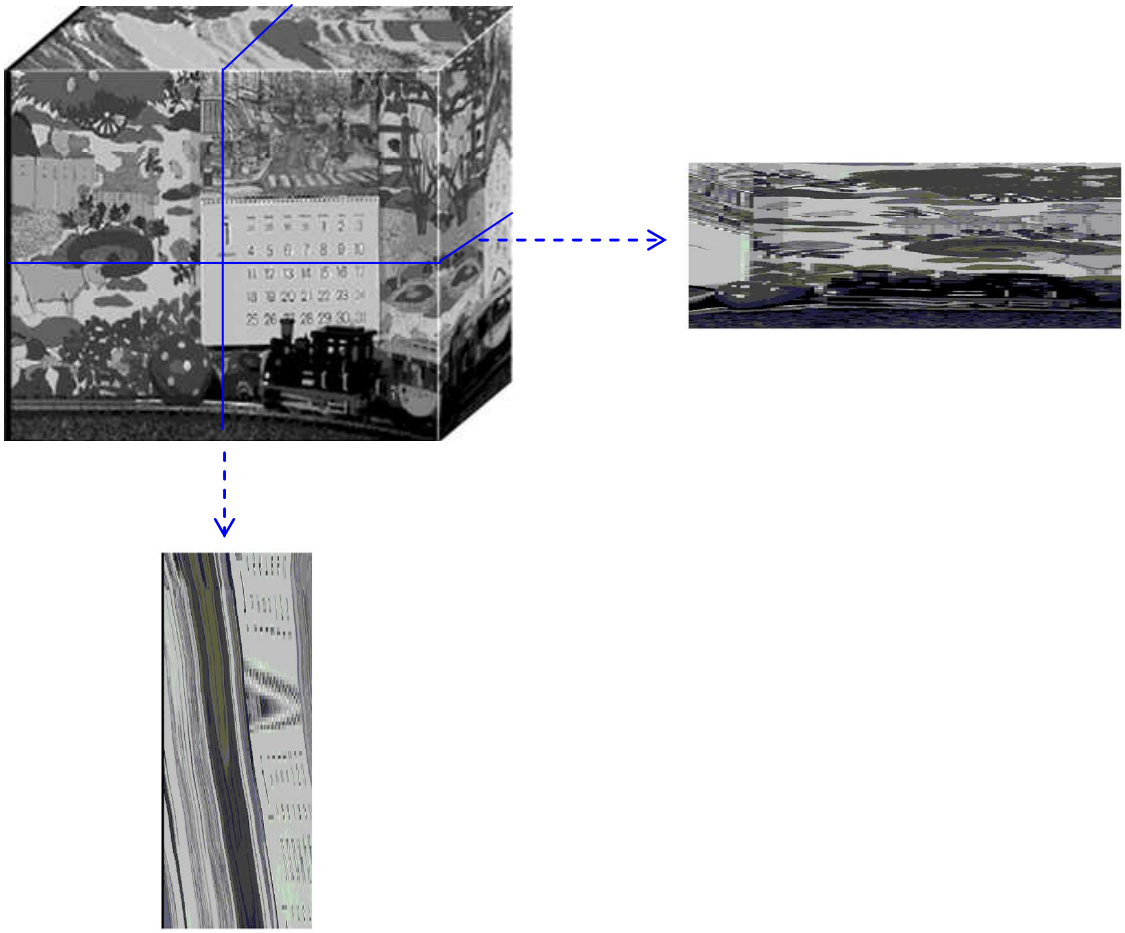

Fig. 18: correlation along time in test sequence "mobile"

To exploit these redundancy, another technique can be used to encode fractally a video. For every frame $i+1$ the domain blocks are searched using the frame i as the searching pool.

The video sequence is first analyzed to find which frames are highly correlated each other. We used a MSE ratio to divide the sequence into group of pictures (GOP) and then use the first frame as a domain pool for the rest of the GOP frames.

Being the GOP composed by p frames, we can encode a sub-sequence stating:

$$S_m' = \bigcup_{i=1}^{p} \tau_i(\mu_0)$$

$$\tau_i : D_1 \to R_i$$

The complete sequence will be $S' = \bigcup_{m=1}^{t} S_j'$ where t the overall amount of GOPs is.

Every frame in the packet is partitioned in range blocks, and a transformation of a domain block obtained by the first frame of the packet is chosen to be the best approximation of every range block on the current frame.

At decoding time the process is inverted and starting from a blank frame, all of the others frame of a packet are reconstructed using the transformation set obtained during the encoding stage.

Even if this method is able to find some of the correlations that exist between frames of a sequence, does not represent an actual extension of the two-dimensional fractal encoding described in the previous chapter. To extend that technique a full three-dimensional approach must be used.

The direct extension of the two-dimensional fractal encoding is to consider the sequence of frames, i.e. the overall sequence, as a three-dimensional object with the third axis represented by the *timing*.

In fractal video coding using the three-dimensional extension range and domain blocks become three dimensional objects: range and domain cubes. The process is straight-forward: the video sequence is partitioned into range and domain cubes, and for every range cube a transformed domain cube is searched to minimize the error measure and to be the best approximation of it.

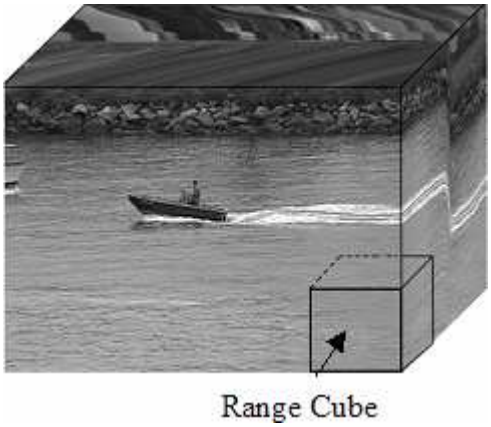

Fig. 19: example of identification of range cube in test sequence "coastguard"

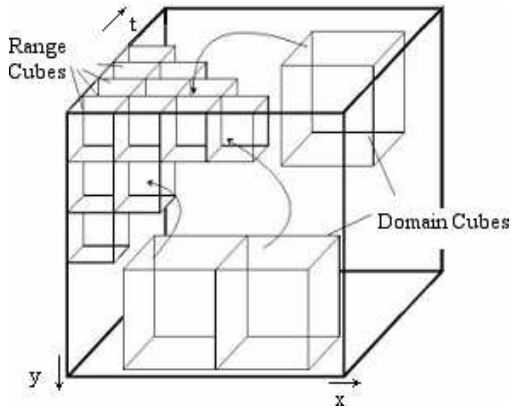

Fig. 20: three dimensional matching process

Since now we work in a three-dimensional space, the number of isometries and affine transformation increase, and a great effort should be made to find some method to speed up the process. This subject will be the focal point of the next section using, as we will see, wavelets decomposition and motion detection.

III.3 Slow motion with fractal expansion

As for image encoding, fractals have some peculiarities when applied on video signals. We saw in chapter 2 that a fractal code extracted from an image can be decoded with a zoom factor.
This quality pushed our study towards the possibility of “zooming” an entire video sequence or a subpart of it.

The problem relies on understanding what an “expansion” of a video signal really means.
Considering the video sequence as a three dimensional object, being X and Y the image plane and T the time axis, we can see that an expansion on the image plane leads to a classical zooming of a frame while the expansion along the time axis increase the “length” of the sequence, meaning that we “add” frames to the sequence.

Keeping the frame rate constant the result is that the sequence is “slowed” down by a factor equal to the expansion factor (i.e. the “zooming” factor).
This means that a fractal expansion applied to a video sequence leads to an “implicit” interpolation between frames and to a “slow motion” effect.
This effect is widely used in commercial devices or as a special FX for media production.

As for image zooming using fractal we prove that the quality of this expansion along time is better than other classical method as polynomial interpolation, spline and motion vector interpolation.

More, since all the information about zooming are kept inside the fractal code, we can obtain several zooming factor during the decoding stage without complicated computation or algorithms. In fact, as for images, a fractal zoom consist mathematically just in a scalar multiplication.

Depending on which fractal encoding technique is used, we can have different ways of expand a sequence using fractals.

One of the methods consists in considering the slices of a sequence along different planes. Considering a sequence of P frames of size $N \times M$, we have these series of slices (Fig. 21):

- P image planes XY of size $N \times M$
- M slices XT of size $N \times P$
- N slices YT of size $M \times P$

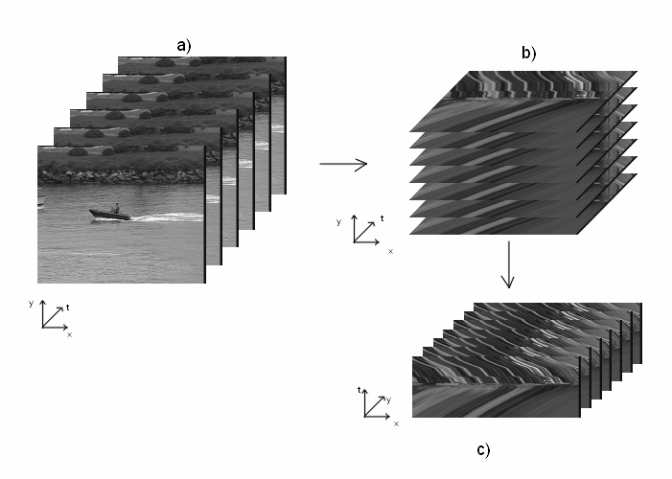

Fig. 21: slices of a video sequence: a) image plane; b) XT; c) YT

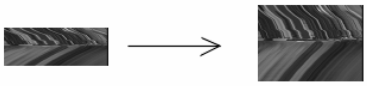

Fig. 22: example of slice (YT) expansion along time axis only

Those slices can be encoded as separate images. Once the slices are encoded a decoding stage with a zooming factor k is applied (Fig. 22). This zooming factor can be applied only along a certain direction (e.g.: the time axis) depending on the fact the final zoom will be only a slow motion or a frame zoom too.

The zoomed slices are then joined together to form the expanded version of the sequence. The joining function (Fig. Fig. 23) we used between the different expanded slices is a simple average value between the pixels on the same position:

$$F'(i,j,p) = \frac{F_{XT}^{j}(i,p) + F_{YT}^{i}(j,p) + F_{XY}^{p}(i,j)}{3} \qquad Eq.\ 3$$

Where:

- F' is the expanded sequence.
- $F_{ZW}^{n}(l,m)$ is the point with coordinates (l,m) of the n-esim element of the series of slices along $ZW \in \{XY, XT, YT\}$

And $1 \le j \le N$, $1 \le i \le M$, $1 \le p \le P$.

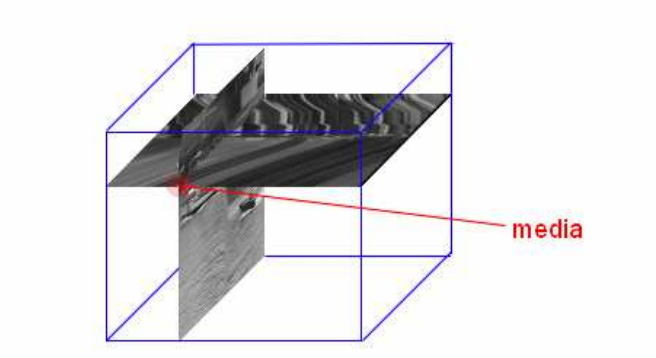

Fig. 23: expansion using slices

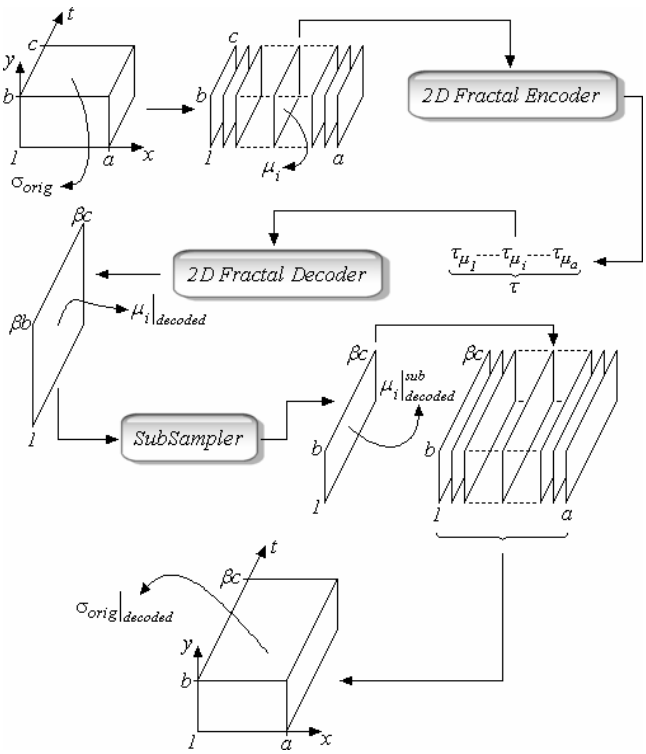

Fig. 24: Sketch of the fractal expansion method using slices

This method leads to good quality for expanded video sequences[2] but has a lot of redundancy: in fact most of the information on slices on a plane is highly correlated with information on other planes.

The full three-dimensional fractal encoding explained in the previous section, leads to the obvious extension of the image zooming obtained in the two-dimensional encoding.

In fact using a full three-dimensional fractal encoder being D and R the size respectively of domain and range cubes, at decoding stage we can obtain an expanded replica (by a factor k) of the original sequence using domain and range cubes of size $k \cdot D$ and $k \cdot R$.

The process is shown in Fig. 25 and Fig. 26.

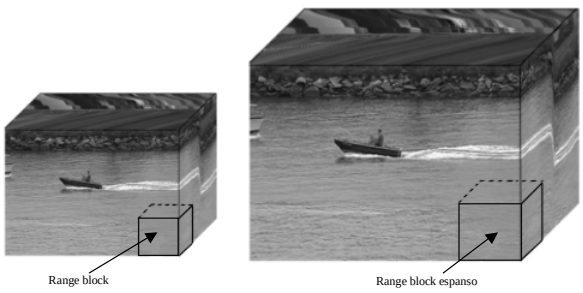

Fig. 25: range cubes example on encoding stage and decoding stage

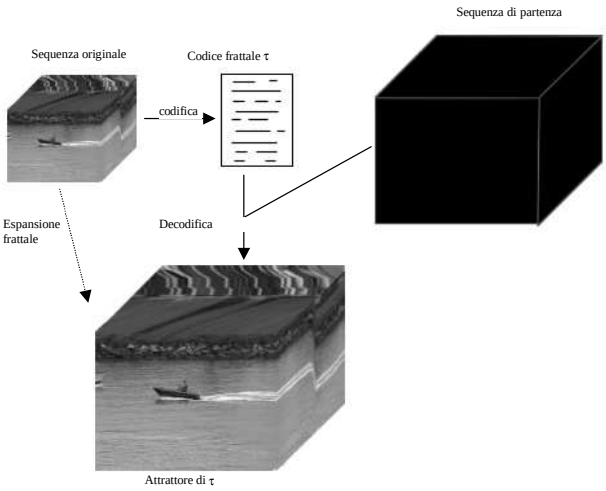

Fig. 26: sketch of full three-dimensional fractal expansion

[2] Quality measures will be shown on section III.4 of this chapter

Using the full three-dimensional encoding and expansion to obtain zoomed replicas of sequence leads to some problems. We can divide these problems in two main groups:

- Visual quality loss
- Computational cost

We developed some techniques to overcome both of these issues.

III.3.A Visual quality improving techniques

Using fractal zoom leads to blockness distortion during the decoding step along both the time and spatial dimensions (image plane). This problem derives from partitioning the original sequence into non overlapping range cubes during the encoding process. When high zoom (i.e. above 8x factor) is performed these artefacts become visible and the overall visual quality decreases.

Even if the origin of this distortion is the same, the effects are different on image plane and time axis.

While on the image plane the effect is the appearance of artefacts on the frame, along the time axis of a “slow motion” sequence the blockness produce an annoying effect known in literature as “jerky motion”.

This jerky motion results in rapid and not natural movements of blocks (i.e.: range blocks in our case) or entire frames along the scene of a video sequence.

We saw in the previous chapter how the problem of blockness distortion could be solved using the O.R.B. and O.S.O. technique for the image zooming using fractals.

In that sense, to enhance the fractal coding visual quality performance, Overlapped Range Blocks (O.R.B.) technique has been extended to the three dimensional case and called Overlapped Range Cube (O.R.C.) partitioning.

Extending [25], eight different partition of the active object and four partitions for the static background are computed. Four different fractal codes for the background and eight for the active object are extracted and coded independently. These partitions correspond to 2D (Fig. 2.3) and 3D (Fig. 2.4) overlapping partition of range blocks and cubes respectively.

			
I	**II**	**III**	**IV**
			
V	**VI**	**VII**	**VIII**

Table 2: ORC intersections

At decoding time, the inverse process is applied, and the fractal zoom is performed. An Ordered Cube Overlapping (O.C.O.) post-process, defined as an extension of Ordered Square Overlapping (O.S.O.), merges the parts created by the overlapped partition of three-dimensional fractal code. The O.S.O. presented in [25] is a windowed median filter that computes the median value from each partition generated by O.R.B. The technique is applied in the three-dimensional case and the O.C.O. computes the median among the eight partitions from the O.R.C.

A drawback of using O.R.C. and O.C.O. is the growth of the computational cost of the fractal coding process.

III.3.B Computational cost reduction

The increasing amount of process time derives not only for the bigger number of isometries but also because of the enormous dimension of the matching space.

In fact a video sequence is usually composed by thousand of frames, and the partitions of range and domain cubes contain a huge amount of items.

For sake of explanation if we have a CIF video sequence[3] composed by 1024 frames (approximately 20 sec. of video @50Hz), using a non-overlapping (to simplify the computation) partition of domain cubes of size 4x4x4 and range cubes of size 2x2x2, this leads to:

- 1.640.448 Domain Cubes
- 13.123.584 Range Cubes

Using a close set of 16 isometries on the three-dimensional space, without considering massive transforms, we have $1.640.448 \times 13.123.584 \times 16 \approx 2,7 \cdot 10^{15}$ as the upper limit of matches' amount.

This number leads to the pratical impossibility of using a raw fractal encoding of a whole sequence, which usually is larger than a CIF frame and longer than just 20 seconds.

To limit the number of matches we decided first to use the same approach defined above, and frames are grouped into packets that are going to be treated as single units. The packet size is chosen according to the temporal activity within the sequence, so that bigger sizes can be selected for slowly changing scenes without a significant time processing increase. This due to the fact that using a threshold to identify one of the combination of domain and transformation that leads to a close representation of a range block, slowly changing scenes usually have a big percentage of exact copies of blocks in the same position (or in the neighbour of the searching area) along time.

Packets are selected considering the temporal variance of the sequence, estimated by means of the Minimum Square Error (MSE) metric between frames:

[3] The size of a CIF (*Common Interchange Format)* frame is 352x288 pixels

$$MSE(h,k) = \frac{\sum_{i=0}^{N-1}\sum_{j=0}^{M-1}\left(F_{i,j}^{h} - F_{i,j}^{h+k}\right)^2}{M \cdot N} \qquad \text{Eq. 4}$$

$$h,k \in [1,2,...n]$$

where $F_{i,j}^{p}$ is the pixel (i, j) of the frame and, p is the frame position within the sequence, $M \cdot N$ the frame size and n the number of frames of the entire sequence.

Among the totality of frames composing the sequence, a certain number of key-frames are selected. A packet is defined as composed by a set of adjacent frames temporally located between two consecutives key-frames, as shown in Fig. 27.

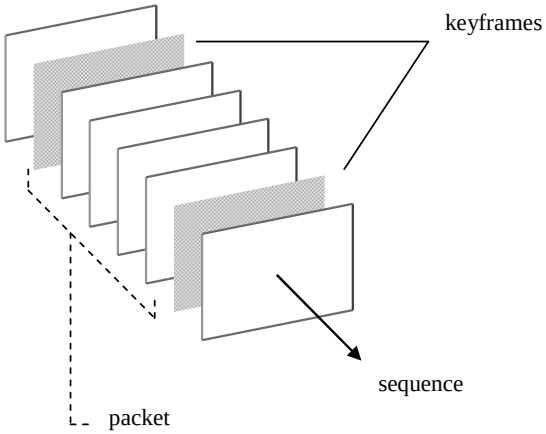

Fig. 27: packetization process

At the beginning of the division process the first frame of the sequence to be expanded is chosen as initial Key-frame.

More in general, once a frame h has been identified as the first key frame for a packet, a successive frame k is marked as the ending key-frame for the packet if

$$MSE(h,k) > Th \qquad \text{Eq. 5}$$

where Th is a threshold selected so that

$$Th = \frac{MSE(1,n)}{2} \qquad \text{Eq. 6}$$

In other words, for each packet the temporal variance must be lower than the 50% of the temporal variance of the whole sequence. Equation Eq. 6 assures at least a two packet subdivision of the sequence to be expanded.

According to Eq. 5 and Eq. 6, each packet can be composed by a variable number of frames. At the end of the packetization process, each packet is considered for coding as a single unit: in this manner the computational load and, thus, the time consumed for the coding are significantly reduced.

However, this packet based coding leads to discontinuity problems when the sequence is zoomed, if each packet is independently coded. In fact, since the expansion is applied within each packet, the successive packet merging process generates a temporal discontinuity between adjacent "zoomed" packets.

To solve this problem, each packet is coded using the motion information of the previous packet as a boundary condition. Owing to this, the presence of a buffer is necessary to assure the process being causal.

A more general constraint is that the packet sizes must be a multiple of R, size of the range block, and not smaller than D, size of the domain block. This guarantees the packet being partitioned into range and domain blocks, and not into portions of them.

An example of right and wrong packetization is shown in Fig. 28.

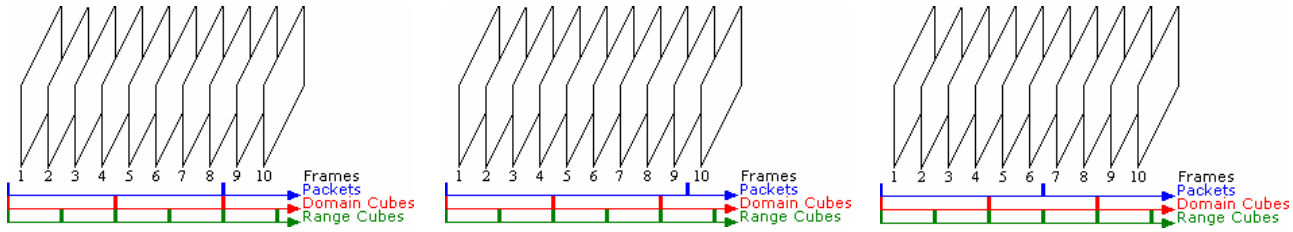

a) b) c)

Fig. 28: example of packetization boundaries: a) right packetization; b) wrong packetization: the number of frames is not multiple of domain or range cube size; c) wrong packetization: the number of frames is multiple only of range cube size but not of domain cube size.

In order to further reduce the computational load and consequently speed-up the coding process, within each packet an active scene detector is used. A "moving object" is defined as a group of three dimensional blocks that have higher temporal variance than the rest of the packet.

To extract the moving object, each frame is divided into tiles of $R \times R$ size to form a partition of range blocks. The MSE among corresponding tiles belonging to different frames is evaluated. If the MSE is higher than a prefixed threshold, tiles are labelled as "motion tiles" and grouped to form a three dimensional moving block.

a) b)

Fig. 29: Motion detection on a range cube. a) no movement found. b) couples (1,5) – (2,6) – (4,8) don't change while on pixels (1,5) and (4,8) there is a color variation along time.

The set of the so extracted blocks identifies the moving object. Remaining tiles are marked as “static” and form a two-dimensional static block referred as “background”. The threshold is selected adaptively averaging the MSE for all tiles composing the packet. The moving object is suited to be encoded with a three-dimensional fractal coder whereas the background is processed with a two-dimensional code. During expansion only the moving object is expanded along the time axis while the static blocks are considered as background information are expanded only on the image plane and displayed unchanged for the whole duration of the packet.

A sketch of the process is shown in Fig. 30.

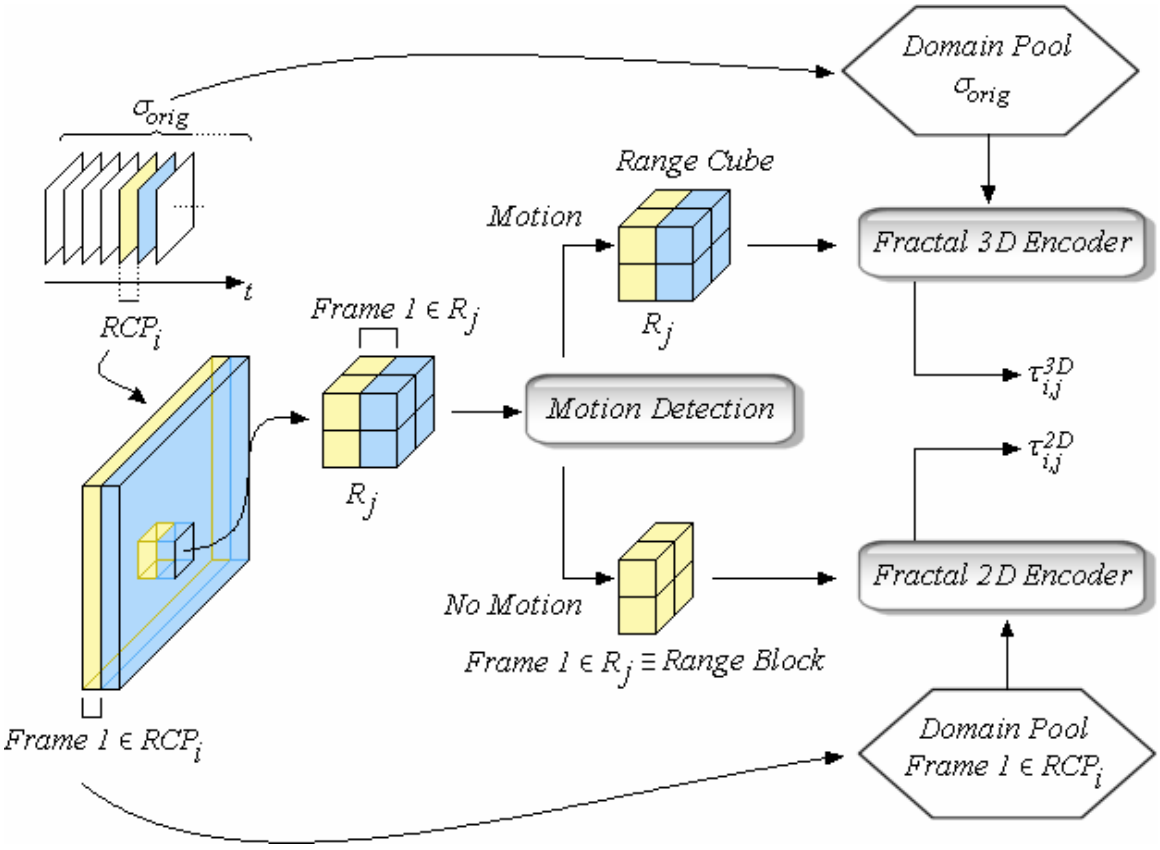

Fig. 30: Hybrid fractal encoder

III.3.C Computational cost reduction using wavelet decomposition

A drawback of using ORB and OCO is the growth of the computational cost of the fractal coding process. To speed up the process, a wavelet based approach [20] is used. For the active object a three dimensional wavelet subband analysis is computed. For the entire low pass component a fractal code is then extracted using ORB partitioning. For the high-pass components, the following coefficients classification procedure is performed [21]: let S_m be the m-th subband; we denote by $\{x_i^m\}$ the wavelet coefficients of S_m and by $p^m(x)$ the histogram of $\{x_i^m\}$. In $p^m(x)$, starting from the maximum $x_{\max}$ and moving to the tails of the distribution (see Fig. 31); two thresholds are identified, that is $t_1^m, t_2^m : \int_{t_1}^{t_2} p^m(x)dx = K, \quad K \in (0,1]$.

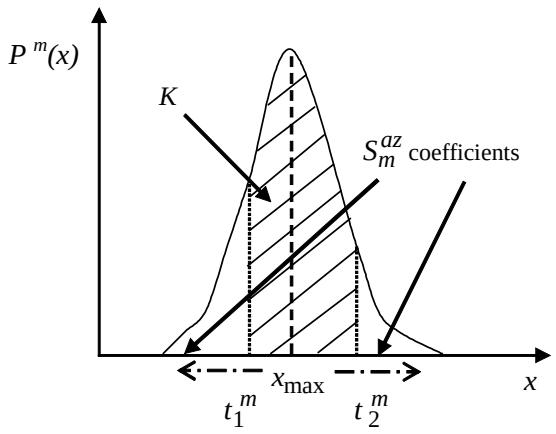

Fig. 31: Wavelet coefficient classification process.

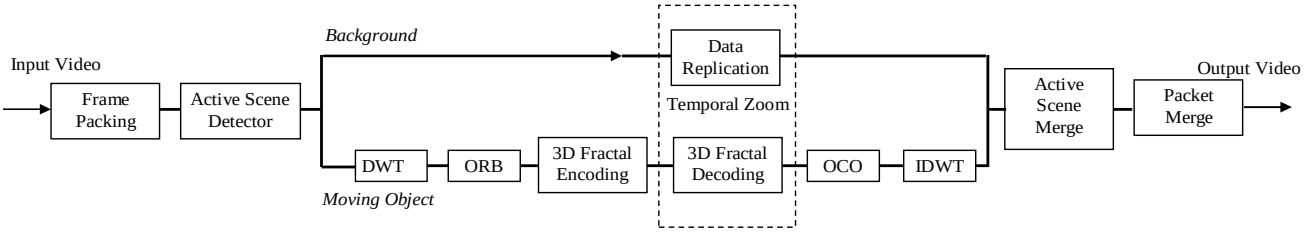

Fig. 32: Flowchart of the proposed method.

These thresholds identify the wavelet coefficients constituting the active zone for S_m, that is $S_m^{az} = \left\{ \forall x \in \left\{ x_i^m \right\}, x \notin \left[t_1^m, t_2^m \right] \right\}$. In other words, an active zone is composed by those coefficients located on the distribution's tails identified by the above thresholds.

After the classification process, a binary-value mask, indicating the position of active zone coefficients within the subband, is extracted. Those coefficients that do not belong to an active zone are discarded, while the S_m^{az} coefficients are ORB partitioned and then fractal encoded.

The K parameter is unique for all the subbands and controls the speed up, and on the other hand, the accuracy of the fractal coding process; higher values of K correspond to higher speed up factors, but also turn out in lower final visual quality achieved.

At decoding stage OSO filtering is applied independently to each subband.

An additional advantage in terms of time saving of wavelet analysis is the “parallelization” of the entire process that increases the speed in a multithreaded environment.

A flowchart of the whole process is depicted in Fig. 32.

III.4 Performance Analysis and Comparison

We tested ([26]) the effectiveness of the proposed method by comparing the result achieved to those obtained, under the same constraint (i.e., equal slow motion factors) by frame replication and classical interpolation techniques.

Test sequences were *Silent*, *Miss America*, *Stefan*, *Carphone, Coastguard* and *Mobile* in CIF format. In a framework of broadcasting digital TV, to measure the quality achieved we refer to the video quality assessment described on [22] and formalized in [23]. As to this, the perception of continuous motion by human vision faculties is a manifestation of complex functions, representative of the characteristics of the eye and brain.

When presented with a sequence of images at a suitably frequent update rate, the brain interpolates intermediate images, and the observer subjectively appears to see continuous motion that in reality does not exist. In a video display, *jerkiness* is defined as the perception, by human vision faculties, of originally continuous motion as a sequence of distinct "snapshots" [23]. Usually, jerkiness occurs when the position of a moving object within the video scene is not updated rapidly enough.

This can be a primary index of a poor performance for a slow motion algorithm. More in general, the total error generated by an incorrect coding of a moving object on a video sequence is representative of spatial distortion and incorrect positioning of the object. In [23] a class of full reference quality metrics to measure end–to–end video performance features and parameters was presented.

In particular, [23] defines a framework for measuring such parameters that are sensitive to distortions introduced by the coder, the digital channel, or the decoder. Ref. [23] is based on a special model, called the *Gradient Model*. Main concept of the model is the quantification of distortions using spatial and temporal gradients, or slopes, of the input and output video sequences.

These gradients represent instantaneous changes in the pixel value over time and space. We can classify gradients into three different types that have proven to be useful for video quality measurement:

- *The spatial information in the horizontal direction* SI_h
- *The spatial information in the vertical direction* SI_v
- *The temporal information* TI .

Features, or specific characteristics associated with individual video frames, are extracted in quantity from the spatial and temporal information. The extracted features quantify fundamental perceptual attributes of the video signals such as spatial and temporal detail. A scalar feature is a single quantity of information, evaluated per video frame.

The ITU recommendation [23] divides the scalar features into two main groups: based on statistics of spatial gradients in the vicinity of image pixels and based on the statistics of temporal changes to the image pixels.

The former features are indicators of the amount and type of spatial information, or edges, in the video scene, whereas the latter are indicators of the amount and type of temporal information, or motion, in the video scene from one frame to the next. Spatial and temporal gradients are useful because they produce measures of the amount of perceptual information, or change in the video scene.

Surprisingly parameters based on scalar features (i.e., a single quantity of information per video frame) have produced significant good correlation to subjective quality measurement (producing coefficients of correlation to subjective mean opinion score from 0.85 to 0.95) [22].

This demonstrates that the amount of reference information that is required from the video input to perform meaningful quality measurements is much less than the entire video frame.

A complete description of all the features and parameters in [23] is beyond the scope of this work.

In the following a brief summary of the above feature will be given, a mathematical determination of the above features is provided in [23]:

Blurring: A global distortion over the entire image, characterized by reduced sharpness of edges and spatial detail.

The [23] defines a Lost Edge Energy Parameter for measuring the blurring-effect, which causes a loss of edge sharpness and a loss of fine details in the output image. This loss is easily perceptible by comparing the Spatial Information (SI) of the output image with the SI of the input image.

The lost edge energy parameter compares the edge energy of the input image with the edge energy of the output image to quantify how much edge energy has been lost.

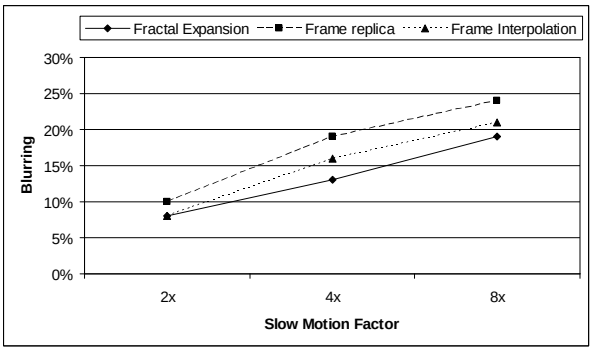

Fig. 33: Measured blurring for "Silent" sequence.

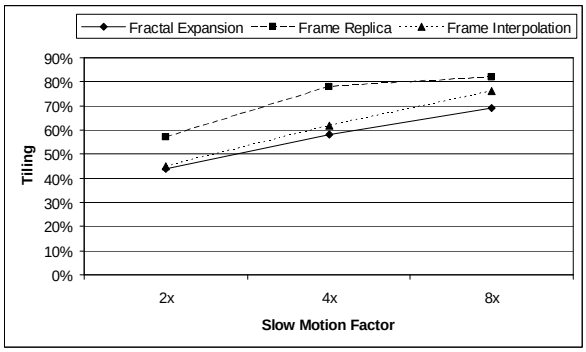

Fig. 34: Measured tiling for "Silent" sequence..

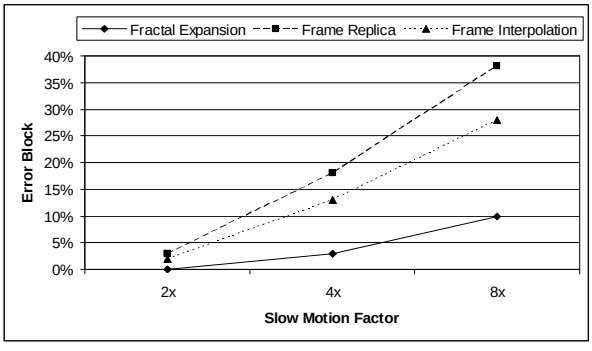

Fig. 35: Measured error blocks for "Silent" sequence.

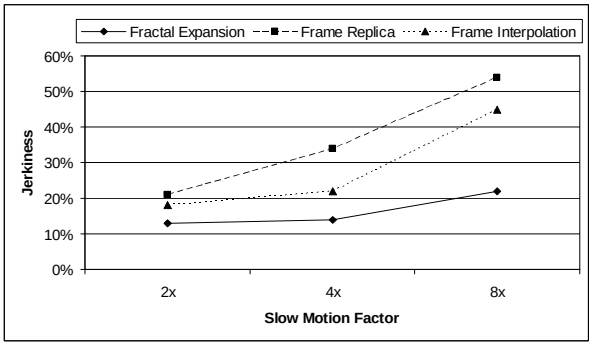

Fig. 36: Measured jerkiness for "Silent" sequence.

Tiling: Distortion of the image characterised by the appearance of an underlying block encoding structure. The [23] paper defines a HV to non-HV edge energy difference parameter for quantifying the tiling impairment.

In contrast to blurring which results in lost edge energy, tiling creates false horizontal and vertical edges. By examining the spatial information (SI) as a function of angle, the tiling effects can be separated from the blurring effects.

Error Block: A form of block distortion where one or more blocks in the image bear no resemblance to the current or previous scene and often contrast greatly with adjacent blocks. Reference [23] defines an Added Motion Energy Parameter for detecting and quantifying the perceptual effects of error blocks.

The sudden occurrence of error blocks produces a relatively large amount of added temporal information. So the Added Motion Energy Parameter compares the temporal information (TI) of successive input frames to the TI of the corresponding output frames.

Jerkiness: Motion that was originally smooth and continuous is perceived as a series of distinct snapshots. Reference [23] paper defines a Lost Motion Energy and Percent Repeated Frames Parameter for measuring the jerkiness impairment. The percent repeated frames parameter counts the percentage of TI samples that are repeated, whereas the average lost motion energy parameter integrates the fraction of lost motion (i.e., sums the vertical distances from the input samples to the corresponding repeated output samples, where these distances are normalised by the input before summing).

To extract the performance metrics we deployed the Video Quality Metric (VQM) software developed by the ITS-Video Quality Research project [24] and compliant with [23]. All tests performed on the different test sequences produced similar outcomes that have been proven to be dependent to the natural temporal activity of the sequences.

Therefore, for the shake of concision, we reported here only a subset of results that were relevant to the *Silent* and *Mobile* sequences. The *Silent* sequence presents a limited temporal activity compared to *Mobile*.

We considered 64 frames for the sequence *Silent* at 15 frame/s rate and 128 frames for the sequence *Mobile* at 30 frame/s rate, both corresponding to approximately 4 seconds of the video scene. Fig. 33 to Fig. 40 show the results of the above mentioned features for the proposed method, the frame replica and the spline cubic interpolation techniques, in case of 2x, 4x and 8x slow motion factors. A general overview of the outcomes shows the advantage in using the proposed technique for higher slow motion factors. An in-depth analysis of the results demonstrates the sensitivity of the method to the natural temporal activity of the sequences. Fig. 33, Fig. 34, Fig. 35, and Fig. 36 show how blurring and tiling distortion for *Mobile* at 2x slow motion factors is lower for frame

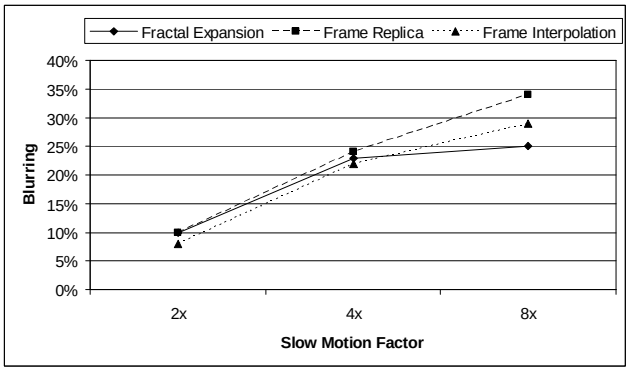

Fig. 37: Measured blurring for "Mobile" sequence.

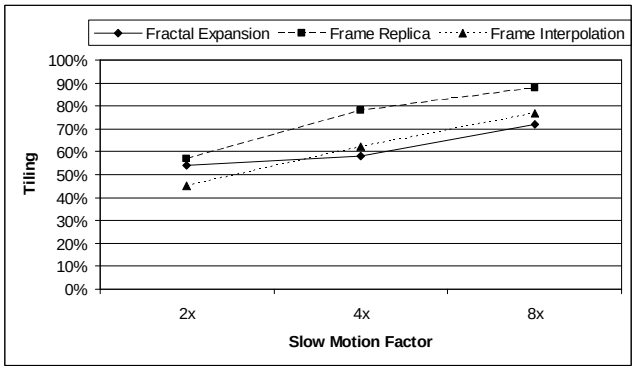

Fig. 38: Measured tiling for "Mobile" sequence.

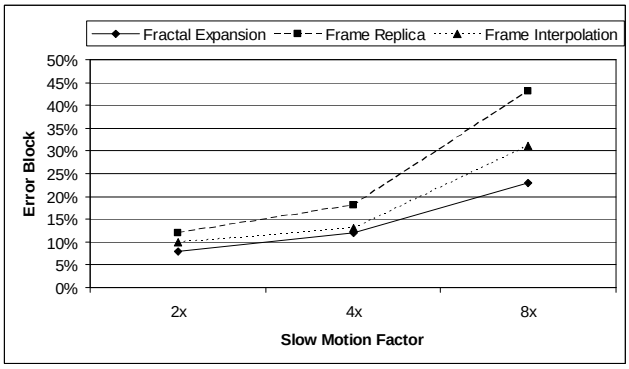

Fig. 39: Measured error blocks for "Mobile" sequence.

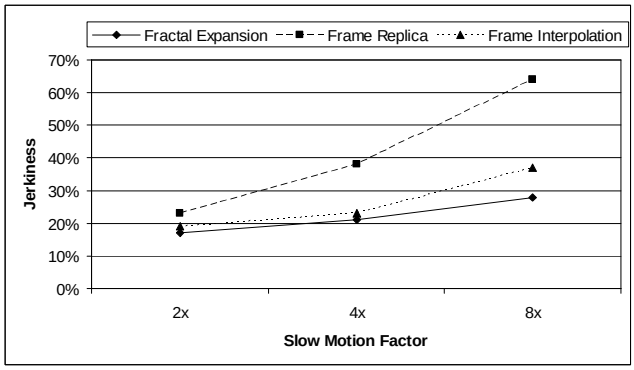

Fig. 40: Measured jerkiness for "Mobile" sequence.

interpolation that for fractal expansion and frame replica, whereas, for *Silent* better spatial distortion performance is obtained by the proposed scheme. For higher slow motion factors the

predominance of the proposed method is more evident and is due to the joint use of motion estimation and ORB/OSO fractal coding that allows mitigating the presence of spatial artifacts.

Fig. 35 shows how for *Silent* the error block feature measured for the proposed system is considerably lower than for frame replica and interpolation for high slow motion factors, whereas is comparable for 2x temporal expansion.

For *Mobile* (Fig. 37) the error block is comparable for 2x and 4x slow motion factors for fractal zooming and interpolation and only for higher slow motion factors the prevalence of the proposed system is noticeable.

This outcome is mainly due to the intrinsic block-based nature of fractal coding that, in presence of high temporal activity within the scene, reduces the efficacy of the proposed approach.

The results shown in Fig. 36 and Fig. 40 are relevant to jerkiness and confirm the above statement: the effectiveness of the proposed method for this feature is evident for *Mobile* (Fig. 40) only for 8x slow motion factor.

For lower temporal expansions the proposed scheme achieves performance comparable to classical interpolation technique.

For *Silent* the predominance of fractal expansion in terms of jerkiness is evident for slow motion factors higher than 2x.

The use of a combined motion and subband analysis during the fractal coding and again the smoothing properties of the OSO filtering allow the method achieving high performance in terms of fluent motion flow during the presentation in slow motion of video sequences.

Chapter IV

Fractals and color image compression

IV.1 Introduction

This chapter proposes a fractal coding technique based on Iterated Function Systems (IFS) to encode color image signals. IFS aim to exploit the redundancy given by the *self-similarity* always contained in natural images.

Exhaustive studies have been conducted on ISF applied to grey level image coding but, on the other hand, even if fractal coding of color images has been investigated, still remain an open issue. The need for color image compression is gaining importance in recent time due to large scale multimedia applications.

Conventional fractal compression schemes can easily be extended to color image compression as a color image is usually represented in multichannels such as Red, Green and Blue (RGB) components.

Thus each channel in color image can be compressed as a grey-level image. Hurtgen, Mols and Simon proposed a fractal transform coding of color images in [27]

This kind of encoding lacks the possibility of considering similarities between the three color planes, thus not achieving a good compression ratio neither a fair population on the domain pool needed to obtain a high quality interpolation for zooming purposes.

To exploit the spectral redundancy in RGB components, the root mean square error (RMS) measure in gray-scale space can be extended to 3-dimensional color space for fractal-based color

image coding [28]. Experimental results show that a 1.5 compression ratio improvement can be obtained using vector distortion measure in fractal coding with fixed image partition as compared to separate fractal coding in RGB images.

However, since RGB space is not perceptually uniform, we decided to use another color space, called CIE-L*a*b*.

Also RMS metrics, as deeply discussed on the other chapters, demonstred to not be a good quality measure, so we introduced a different metric never use for fractal encoding purpouses, called Earth Mover's Distance Metric.

We then will propose a novel approach for coding color images based on the joint use of the Lab color space and Earth Mover's Distance (EMD) measure [30]

EMD has been suitably deployed for color image retrieval applications and can be thought as a vector metric that combines spatial and color information to resolve similarities among color images. This definition clearly gave us some hints on how this metric was extremely suitable for fractal encoding, which is, after all, a *search* of similarities among *parts of an image*.

In this work we implement a fractal coding approach that relies on EMD for finding self-similarities within color images represented in the Lab color space and later we show some results of this technique.

IV.2 The CieLAB color space

A color space is a mathematical representation of a set of colors. The three most popular color models are RGB (used in computer graphics), YIQ, YUV or YCbCr (used in video systems) and CMYK (used in color printing).

However, none of these color spaces are directly related to the intuitive notions of hue, saturation and brightness, which are the basis of our color perception.

This resulted in the temporary pursuit of other models, such as HSI and HSV, to simplify programming, processing and end-user manipulation but trying to get closer to the actual representation of colors in our brain.

Indeed, mathematically, all of the color spaces can be derived from the RGB information supplied by devices such as cameras and scanners.

The red, green and blue (RGB) color space is widely used throughout computer graphics, since Red, green and blue are three primary additive colors (individual components are added together to form a desired color) and are represented by a three-dimensional, Cartesian coordinate system.

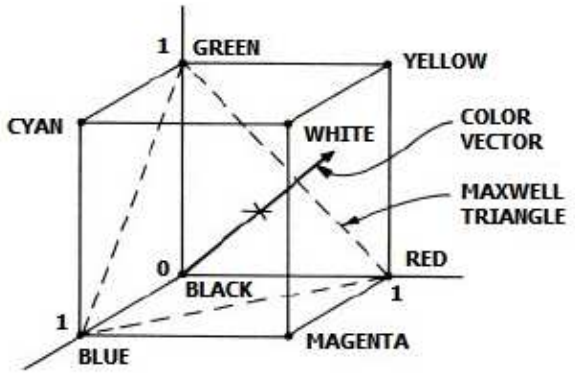

Fig. 41: The RGB color space representation. The triangle, called Maxwell triangle has been drawn between the three primaries. The intersection point of a color vector with the triangle gives an indication of the hue and saturation of the color in terms of the distances of the point from the vertices of the triangle.

The RGB color space is the most prevalent choice for computer graphics because color displays use red, green and blue to create the desired color. Therefore, the choice of the RGB color space simplifies the architecture and design of the system.

Also, in a system that is designed using the RGB color space can take advantage of a large number of existing software routines, since this color space has been around for a number of years.

However, RGB is not very efficient when dealing with “real-world” images. All three RGB components need to be of equal band width to generate any color within the RGB color cube. The result of this is a frame buffer that has the same pixel depth and display resolution for each RGB component.

Also, processing an image in the RGB color space is usually not the most efficient method. For example, to modify the intensity or color of a given pixel, the three RGB values must be read from the frame buffer, the intensity or color calculated, the desired modifications performed and the new RGB values calculated and written back to the frame buffer. If the system had access to an image stored directly in the intensity and color format, the processing steps would be faster.

For these and other reasons, many video standards decided to use luminancy and two color difference signals. The most common systems are the YUV and YCbCr color spaces.

The YUV color space is used by the PAL (Phase Alternation Line), NTSC (National Television System Committee), and SECAM (Sequentiel Couleur Avec Mémoire) composite color video standards. The black-white system used only luminancy (Y) information;

This system was ideated mainly for backward compatibility with old monocromatic television, since U and V where easily be discarded by old equipment.

Color receivers decoded the additional color information to display a color picture. The equations that describe the direct transformation RGB → YUV are:

$$Y = 0.299R + 0.587G + 0.114B$$
$$U = -0.147R + 0.289G + 0.436B = 0.492(B - Y)$$
$$V = 0.615R - 0.515G - 0.100B = 0.877(R - Y)$$

and for the inverse transformation:

$$R = Y + 1.140V$$
$$G = Y - 0.395U - 0.581V$$
$$B = Y + 2.032U$$

For digital RGB values with a range of 0-255, Y has a range of 0-255, U a range of 0 to ±112 and V a range of 0 to ±157.

As the RGB color space, the YUV space is not uniform concerning the HVS.

A system is said to be not uniform if a little perturbation of a value is perceived linearly along the possible variation of that value. This means that a color space is perceptually uniform if a distance from a color a and another color $b = a + \Delta c$ will be perceived as constant independently from a or b. Using a non perceptually uniform space as RGB has the drawback that the Human Vision System will be affected by computer measures for digital video processing, since the distance from RGB value will not be uniform in respect of the HVS.

Starting from these considerations, the Commission Internationale d'Eclairage (CIE) defined a uniform color model, called L*a*b* that represents all the color humans is able to resolve.

Danciu and Hart [29]presented a comparative study of fractal color image compression in the L*a*b* color space with that of Jacquin's iterated transform technique for 3-dimensional color. It has been shown that the use of uniform color space yield compressed images to have less noticeable color distortion than other methods.

Since there are three types of color photoreceptor cone cells in the retina, each with a different spectral response curve, all colors can be completely described by three numbers, corresponding to the outputs of the cone cells.

The CIE workgroup then defined XYZ tristimulus values, where all visible colors can be represented using only positive values of X, Y and Z.

For applications where it is important to be able to measure differences between colors in a way that matches perceptual similarity as good as possible the perceptually uniform color spaces find their best field of use.

The CIE-L*a*b* (CIE-Lab) color space was designed such that the perceived differences between single, nearby colors correspond to the Euclidean distance of the color coordinates.
The (nonlinear) conversions from RGB to CIE-Lab are given by:

$$\begin{bmatrix} X \\ Y \\ Z \end{bmatrix} = \begin{bmatrix} 0.412453 & 0.357580 & 0.180423 \\ 0.212671 & 0.715160 & 0.072169 \\ 0.019334 & 0.119193 & 0.950227 \end{bmatrix} \cdot \begin{bmatrix} R \\ G \\ B \end{bmatrix}$$

$$L^* = \begin{cases} 116\left(\frac{Y}{Y_n}\right)^{\frac{1}{3}} - 16 & if\ \frac{Y}{Y_n} > 0.008856 \\ 903.3\left(\frac{Y}{Y_n}\right) & otherwise \end{cases},$$

$$a^* = 500\left(f\left(\frac{X}{X_n}\right) - f\left(\frac{Y}{Y_n}\right)\right) ,$$

$$b^* = 200\left(f\left(\frac{Y}{Y_n}\right) - f\left(\frac{Z}{Z_n}\right)\right) ,$$

where,

$$f(t)=\begin{cases} t^{\frac{1}{3}} & if\ \dfrac{Y}{Y_n} > 0.008856 \\ 7.787+\dfrac{16}{116} & otherwise \end{cases}$$

and, following ITU-R Recommendation BT. 709 [31] , D65 was used as the reference white point, so that:

$$\begin{bmatrix} X_n & Y_n & Z_n \end{bmatrix} = \begin{bmatrix} 0.95045 & 1 & 1.088754 \end{bmatrix}$$

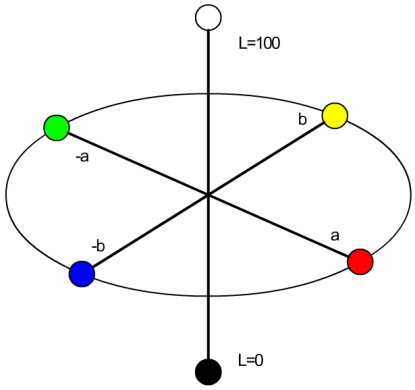

Fig. 42: The CIE-Lab color space representation. Luminance varies from 0 (black) to 100 (white) and a and b components vary from -50 to 50 and represent the color variation along the red-green and blue-yellow axis.

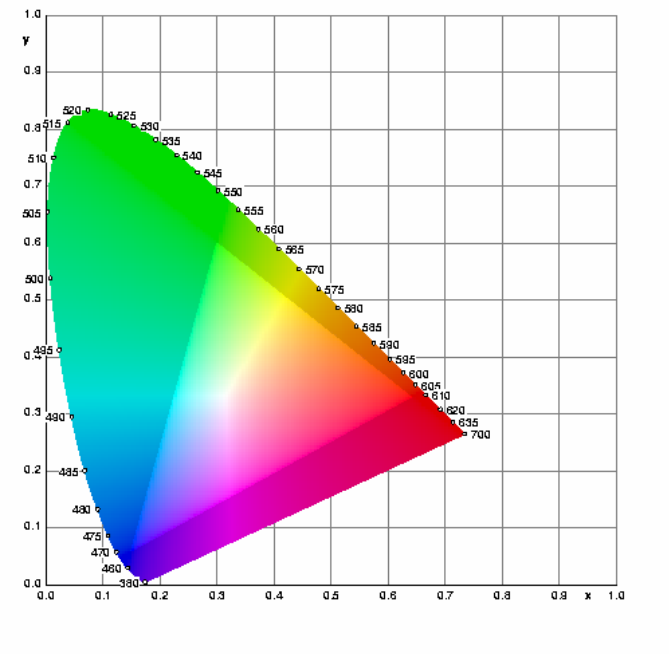

Fig. 43: The CIE-Lab color space.

IV.3 Clustering

An image block signature is a set of features extracted by means of a clustering process. The Clustering tecnique is a branch of Image (or data) segmentation field. A segmentation of an image entails the division or separation of the image into regions of similar attribute. The most basic attribute for segmentation is image luminance amplitude for a monochrome image and color components for a color image. Image edges and texture are also useful attributes for segmentation. Clustering aiming at partitioning the image block in a set of sub regions, (i.e., clusters) formed by pixels gathered according to some distance rule, which is the “segmentation” similar attribute. To each cluster is associated a feature representative of the cluster.

The clustering segmentation concept is simple but usually computationally intensive. Considering a vector $x = [x_1, x_2, \cdots, x_N]^T$ of measurements at each pixel coordinate (j,k) of the image. The measurements could be point multispectral values, point color components and derived color components or neighborhood feature measurements. Is the measurement set is to be effective for image segmentation, data collected at various pixels within a segment of common attribute should be similar. That is, the data should be tightly clustered in an N-dimensional measurement space. If this condition holds, the segmenter design task becomes one of subdividing the N-dimensional measurement space into mutually exclusive compartments, each of which envelops typical data clusters for each image segment. Fig. 44 illustrates the concept for two features. In the segmentation process, if a measurement vector for a pixel falls within a measurement space compartment, the pixel is assigned the segment name or label of that compartment.

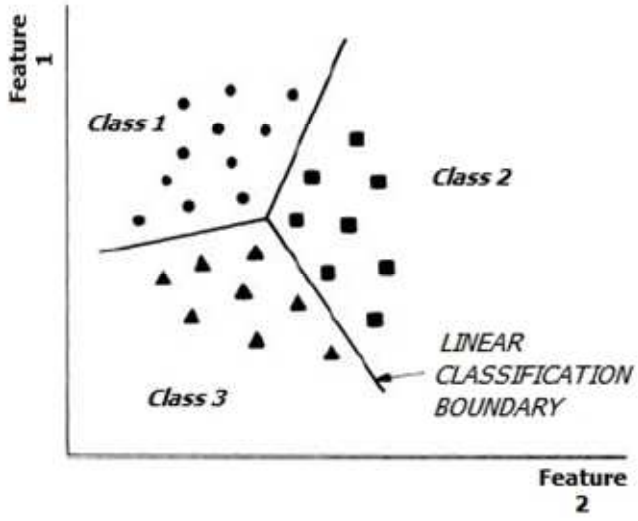

Fig. 44: Data clustering for two feature measurements

The K-Means algorithm is one of the simplest unsupervised learning algorithms that solve the clustering problem. The procedure follows a simple and easy way to classify a given data set through a certain number of clusters (k clusters) fixed a priori. The main idea is to define k centroids, one for each cluster. These centroids should be placed in a cunning way because the result of the algorithm depends largely on the initial centroid positions. The better, immediate choice would be to place them as much as possible far away from each other. The next step is to take each point belonging to a given data set and associate it to the nearest centroid. When no point is pending, the first step is completed and an early grouping is done. At this point, the new k centroids need to be recalculated as barycenters of the clusters resulted form the previous step.

After the new centroids are obtained, a new biding has to be done between the same data set points and the nearest new centroid. A loop has been generated this way; as result of this loop, the k centroids change their location step by step until no more changes occur.

The aim of the algorithm is that of minimizing an objective function, such as a squared error function:

$$J = \sum_{j=1}^{k} \sum_{i=1}^{n} \left\| x_i^{(j)} - c_j \right\|^2 \qquad ,$$

where $\left\| x_i^{(j)} - c_j \right\|^2$ is a chosen distance measure between a data point $x_i^{(j)}$ and the cluster centre c_j and is an indication of the distance of the n data points from their respective cluster centres.

The algorithm can be synthesised as follows:

1. *Place K points into the space represented by the objects that are being clustered. These points represent initial group centroids.*
2. *Assign each object to the group that has the closest centroid.*
3. *When all objects have been assigned, recalculate the values of the K centroids.*
4. *Repeat Steps 2 and 3 until the centroids no longer change. This produces a separation of the objects into groups from which the metric to be minimized can be calculated.*

IV.4 Clustering process applied to fractal encoding

The aim of our study was pratically to use clustering tecniques as hint on similarities between range and domain blocks.

Instead of using one-to-one pixel distance of transformed domain, we wanted to compute distance, i.e. similarity, of blocks using a higher level concept.

To apply clustering to fractal encoding we also needed two other steps: find a way to catalog clusters on domain and range blocks, and an effective way to compute the distance between these objects.

While the second problem is addressed in the next chapter, we define here the concept of the "signature" of an image.

After the clustering properties we use the information gained to create a "signature" of blocks, and compare them each other to find the best approximation of transformed domains for every range block, as usual in the fractal encoding.

Formally, given an image block C of size n, we define its signature as $S(C) = \{(c_j, w_j)\}_{j=1}^{T}$, with T number of clusters, w_j weight and c_j centroid (i.e., the representative element) of the cluster j.

We have now to measure the distance among pixels both in the spatial and color domains. As to the spatial domain, for every pixel $\{y_i\}_{i=1}^{n}$ we limit the search area to a circle centered in y_i with radius *r*. The length of *r* is computed considering the medium spatial distance between y_i and the initial distribution of centroids.

The initial set of 12 centroids for a 8×8 size image block is shown in Fig. 45 while an example of circle bounded search is given in image Fig. 46.

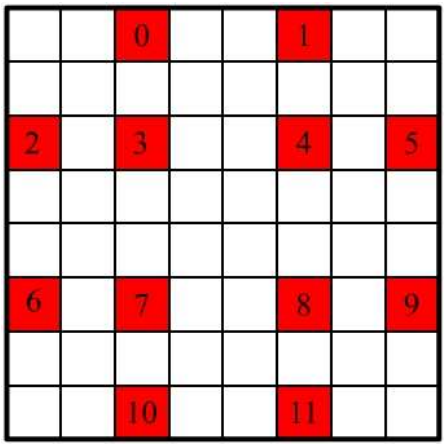

Fig. 45: Initial displacement of centroids.

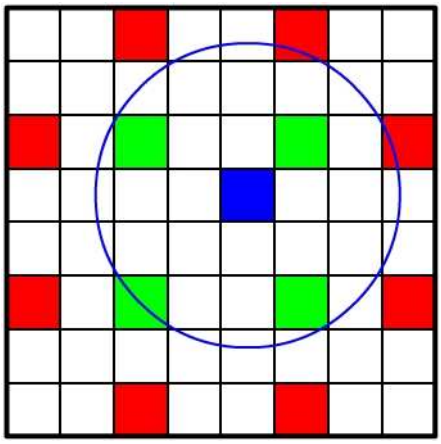

Fig. 46: Circle containing centroids that can be identifyed by element (5,4)

The color distance is also upper bounded by the resolution of the HVS in the uniform color L*a*b* space (HVS_{res}), that is the minimum distance in the L*a*b* color space that allows the HVS discriminating two different colors.

Formally, we define the distance between the generic pixel y_i and a centroid c_j as:

$$\begin{cases} \mathbf{d}(y_i, c_j) = \sqrt{\mathbf{dis}_s^2(y_i, c_j) + \mathbf{dis}_c^2(y_i, c_j)} \\ \mathbf{dis}_s(y_i, c_j) = \dfrac{\left\| y_i - c_j \right\|_{spatial}}{r} < 1; \quad r = \dfrac{1}{T}\sum_{j=1}^{T} \left\| y_i - c_j \right\|_{spatial} \\ \mathbf{dis}_c(y_i, c_j) = \dfrac{\left\| y_i - c_j \right\|_{L^*a^*b^*}}{HVS_{res}} < 1 \end{cases} \quad (1)$$

where $\mathbf{dis}_s(y_i, c_j)$ and $\mathbf{dis}_c(y_i, c_j)$ are their normalized Euclidean distances in the spatial domain and in the L*a*b* color space, respectively. It is worth noticing that $\mathbf{d}(\cdot,\cdot)$ is non negative, symmetric and satisfies the triangle inequality – thus we really work with a metric space.

The clustering process associates y_i to c_j according to:

$$\mathbf{d}(y_i, c_j) = \min_j \mathbf{d}(y_i, c_j)$$

The initial position of the centroids is chosen to be invariant to the possible affine transformation τ performed by the fractal coding. This assures that, given a block signature $S(C)$ and a transform τ, $\tau\left[S(C)\right] = S\left[\tau(Q)\right]$

The number of centroids T is chosen as to satisfy two constraints: maximum uniformity in the distance among centroids; invariance to the geometrical affine transformations (i.e., isometries).

This positioning is spatially homogenous while the distance between centroids as well as the distance between pixel and surrounding centroids is essentially constant. This displacement is invariant as to the 8 possible isometries. At the end of the clustering process a signature is assigned to each range and domain block.

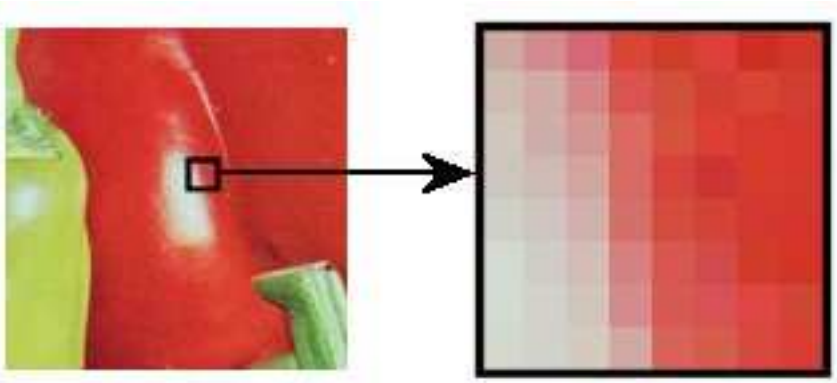

Fig. 47: Block extraction for clustering segmentation

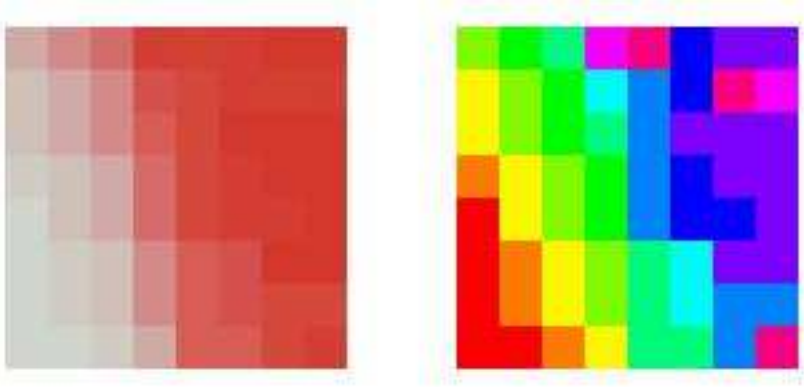

Fig. 48: First segmentation step using CieLab space (colors have been enhanced to clearly identify different clusters)

Fig. 49: Initial clustering

Fig. 50: Searching for centroids of element (0,0)

IV.5 Earth mover's distance for IFS

Now that we have defined a signature of a block, we need a tool to objectively compare them.

The matching process we deployed uses the Earth Mover's Distance (EMD) [33] .EMD is a useful and extendible metric distance, developed by the Stanford Vision Laboratory (SLV), based on the minimal cost that must be paid to transform one signature into another.

The EMD is based on the *transportation problem* from linear optimization, also knows as the Monge-Kantorovich problem [34]. Suppose that several *suppliers*, each with a given amount of goods, are required to supply several *consumers*, each with a given limited capacity. For each supplier-consumer pair, the cost of transporting a single unit of goods is given.

The transportation problem is then to find a least expensive flow of goods from the suppliers to the consumers that satisfy the consumers demand.

Signature matching can be naturally cast as a transportation problem by defining one signature as the supplier and the other as the consumer, and by setting the cost for a supplier-consumer pair to equal the *ground distance* between an element in the first signature and an element in the second.

The ground distance is defined as the distance between the basic features that are aggregated into the signatures. Intuitively, the solution is then the minimum amount of "work" required transforming one signature into the other.

Formally the EMD is defined as a linear programming problem: let P,Q be two image blocks and $S(P)=\{(p_h,w_h)\}_{h=1}^{N}$, $S(Q)=\{(q_k,w_k)\}_{k=1}^{M}$ their signatures with N and M clusters respectively; let d_{hk} be the ground distance between two centroids p_h and q_k, and let f_{hk} the flow between p_h and q_k, defined as the amount of weight of p_h matched to q_k, we want to find a flow that minimizes the overall cost:

$$\mathrm{WORK}\left[S(P), S(Q), f_{hk}\right] = \sum_{h=1}^{N}\sum_{k=1}^{M} d_{hk} \cdot f_{hk}$$

with the following constraints:

$$\begin{cases} f_{hk} \geq 0 \qquad 1 \leq h \leq N, 1 \leq k \leq M \\ \sum_{k=1}^{M} f_{hk} \leq w_h \qquad 1 \leq h \leq N \\ \sum_{h=1}^{N} f_{hk} \leq w_k \qquad 1 \leq k \leq M \\ \sum_{h=1}^{N}\sum_{k=1}^{M} f_{hk} = \min\left(\sum_{h=1}^{N} w_h, \sum_{k=1}^{M} w_k\right) \end{cases} \tag{1}$$

The first constraint assures for unidirectional supplies transportation from $S(P)$ to $S(Q)$. With the second we limit the amount of supplies that can be sent by the clusters in $S(P)$ to their weights.

The third constraint allows the clusters in $S(Q)$ to receive no more supplies than their weights, while the last constraint forces to move as much supplies as possible.

We call this amount the total flow. Once the transportation problem is solved, and we have found the optimal flow f_{hk}, the EMD is defined as the work normalized by the total flow:

$$\mathrm{EMD}[S(P), S(Q)] = \frac{\sum_{h=1}^{N}\sum_{k=1}^{M} d_{hk} \cdot f_{hk}}{\sum_{h=1}^{N}\sum_{k=1}^{M} f_{hk}} \tag{2}$$

The normalization is needed when the two signatures have different total weight, to avoid giving more importance to smaller signatures. In general, the ground distance d_{hk} can be any distance and will be chosen according to the problem at hand.

We need then to define a ground distance that matches our purposes. For the extraction of range and domain blocks signatures we deploy a clustering process based on a metric distance as defined in eq. (1).

Such a distance was a Euclidean based metric able to compare pixels and centroids both in the spatial color domains. The comparison is restricted in the spatial domain by r, which is the medium spatial distance between pixels and the initial distribution of centroids.

In the color space the search is limited to the centroids that differ less than the resolution of the human visual system (i.e., the HVS_{res}). To define the ground distance d_{hk}, we use a similar, but slight different approach. Although we still keep the boundary for the color component, and we use the HVS_{res} value to normalize the Euclidean metric, we do not have elements to limit the search area in the spatial domain.

Therefore, in the spatial domain, we do not set any constraint; we just normalize the distance component to the maximum measured Euclidean distance between centroids. Moreover, in a matching process based on signatures as above defined, to the success of the search, the importance of the spatial component is not the same as the relevance the color component. In fact, in two image blocks having a similar color distribution, the color position can be very different and this can lead to a weak best match algorithm. As to the above considerations, we propose the following measure for the ground distance:

$$\begin{cases} d_{hk} = \sqrt{\lambda \mathbf{dis}_s^2(p_h, q_k) + (1-\lambda)\mathbf{dis}_c^2(p_h, q_k)} \\ \lambda \in \square, \quad 0 < \lambda < 1 \end{cases} \qquad (3)$$

where $\mathbf{dis}_s(\cdot,\cdot)$ and $\mathbf{dis}_c(\cdot,\cdot)$ are the same as in eq. (1), but for the former, here, $r = \max_{h,k} \| p_h - q_k \|_{spatial}$. In fact, the parameter λ in eq. (3) weights the importance given to the color distance respect to the spatial distance and it is chosen as to maximize the quality in the

reconstructed image. It is worth remarking that also d_{hk}, as well as $\mathbf{d}(\cdot,\cdot)$ of eq. (2), is non-negative, symmetric and satisfies the triangle inequality, hence it is a true metric.

To extract the fractal code, IFS look for similarities between range and domain blocks by comparing their signatures. IFS work with contractive transformations reducing the size of the domain blocks to the one of the range blocks.

Therefore, the matching process compares signatures of same total weight. In this case, since the ground distance d_{hk} is a true metric, also the EMD as to eq. (2) defines a metric space. Moreover, it can be shown that in this particular case,

$$\begin{cases} \mathrm{EMD}[S(P),S(Q)] < d_{pq} \\ p = \dfrac{1}{w}\displaystyle\sum_{h=1}^{N} w_h p_h \\ q = \dfrac{1}{w}\displaystyle\sum_{k=1}^{N} w_k q_k \\ w = w_p = w_k \end{cases} \tag{4}$$

where w is the total weight of the two signatures and p,q their average centroids. In other words, the ground distance between the average centroids of two signatures of same total weight is a lower bound for the EMD between the two signatures.

This property is used by the IFS process to reduce the complexity of the similarities search algorithm. Using the EMD for the IFS best matching search has several advantages. In fact, comparing summary information of image blocks extracted by a clustering process leads to an increased robustness of the search process to the offset errors. This is not true for the pixel based RMS approach. Moreover, it is less sensitive to quantization errors due to the intrinsic “averaging” nature of the clustering process.

IV.6 Experimental Results

We tested the effectiveness of the proposed approach by fractal coding several test RGB color images of 512×512 size, coded at 24 bpp.

We compared the achieved results with those obtained by a classic IFS coding, as defined by Jaquin, that implements the similarity search using a RMS measure. Such as benchmark coder performs the coding of the three RGB color planes separately, thus producing three different fractal codes.

Fig. 51: Lena 512x512 coded with RMS-based coder (CR=53, PSNR=29.4 dB).

Fig. 52: Lena 512x512 coded with EMD-based coder (CR=53, PSNR=31.1 dB).

At decoding stage, each so extracted codebook information is independently used to recompose the corresponding color plane. Finally, the color planes are rearranged to form the output image.

In this experimentation we selected 8×8 size range blocks and 16×16 size domain blocks. Therefore, due to the IFS contractive transformation, the block signatures deployed by the search algorithm are composed by clusters of 12 elements.

The initial displacement of the centroids is the one above shown in Fig. 45.

Several tests have been carried out on different test images. We assessed reconstructed image quality in terms of the Mean Squared Error (MSE) that we expressed in terms of the Peak Signal to Noise Ratio (PSNR).

We will comment here results obtained for “Lena”, while some other result are showed in the graph below and not commented.

Due to the choice made for range and domain blocks size, both the compared coding schemes achieved a compression ratio (CR) of about 53.

Fig. 51 and Fig. 52 show the reconstructed images coded with the classic RMS based as described by Jaquin, and with the proposed method. It is noticeable gain of 1.7dB in the PSNR when the EMD based coding is performed.

Fig. 53a) and Fig. 53b) show a detail of the test image displayed in Fig. 51 and Fig. 52, respectively. Some errors due to misinterpretation of color differences during encoding can be noticed. In fig. 5a the border of Lena’s hat is distorted and false colors can be observed. This problem is almost imperceptible in Fig. 53b) where the proposed method based on EMD metric is applied. Colors are, in fact, correctly interpreted and the overall quality is superior.

This outcome is mainly due to the averaging properties of the EMD. In fact, EMD compares clusters and is more resilient to isolated errors at pixel level compared to classic pixel based comparison methods such as RMS.

a) b)

Fig. 53: Detail of “lena” coded with a classic MSE-based coder (a) and with the proposed method (b).

The good interpretation of colors when EMD is used leads also to increase the probability of right interpretation of edges on the images. Basically, with the benchmark RMS-based coder, if an edge is present in one or two color planes, the corresponding detection on the remaining plane will be low, and the block, in that plane, will be considered as a shade area.

Therefore, the overall recognition of the edge will fault and the quality will decrease on the output image. Due to a more precise color and block identification, the EMD-based codec allows overcoming this issue.

Some other results obtained are shown on table 3.

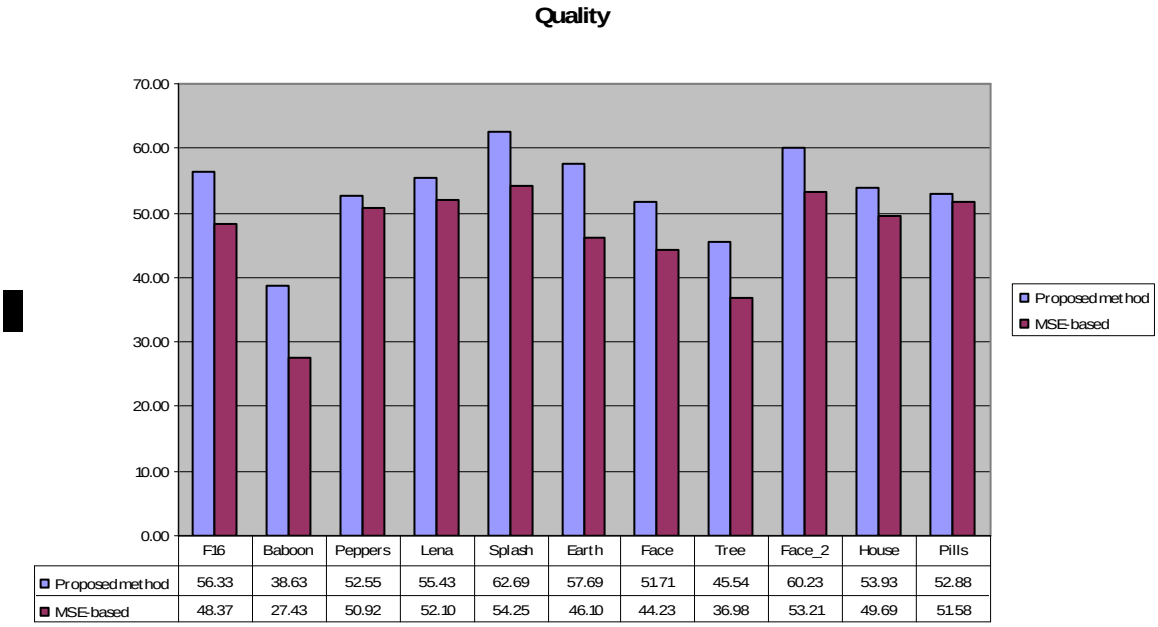

	F16	Baboon	Peppers	Lena	Splash	Earth	Face	Tree	Face_2	House	Pills
Proposed method	56.33	38.63	52.55	55.43	62.69	57.69	51.71	45.54	60.23	53.93	52.88
MSE-based	48.37	27.43	50.92	52.10	54.25	46.10	44.23	36.98	53.21	49.69	51.58

Table 3: PSNR results of proposed method compared to classical MSE (RMS) method.

Chapter V

Conclusions

In this work we proposed two different way of using fractal on different fields, image and videos, but with a lot of points in common.

Fractal theory is a powerful tool we have not only for compressing these signals, but because it opens a wide range of interesting features.

The possibility of using fractal coding more on the “decoding” side, i.e. after a video or an image is downloaded, demonstrated how this tecnique is extremely good to interpolating data available and obtain zoom, slow motion sequences or frame rate conversions.

There are two main innovations we made on the way of encode signals using fractals.

The first one, related to video sequences, is the joint use of several instruments that made possible obtain high quality versions of interpolated sequences. The combination of fractal with wavelet decomposition and moving estimation was successfull, and push us to continue exploring this path.

A great problem when considering interpolated replicas of data is how to measure the quality. The problem is in a certain way a philosophical issue since we want to measure how good is data we obtain compared to data we do not have before.

Some escamotages as first subsample video sequences and after the decoding obtain a full scale video to be compared with the original one, are, as we said just escamotages, especially when using objective measures as RMS, that made a low level simple computation between pixel values instead of measuring the overall high level quality as our brain make.

In this scenario we adopted brand new metrics as the ITU-R BT-1683 [23] metric, which gave us a more powerful amount of measures that can address our needs.

The other main innovation we made was in the encoding of images.

By always focusing on high level quality and our aim (using fractals to interpolate data), we introduced a different approach on the usual way of fractally encode images.

The use of Earth Mover's Distance on fractal encoding is original, and the joint use of EMD with clustering and signature extraction made possible to obtain good results for color images.

As we said at the beginning of this work, fractals have innumerable way of use. The results obtained in our research demonstrated that a lot of innovation can still be done in this field.

In fact future works can include the use of EMD and clustering also on encoding video sequences, while instead the use of ORB and OSO can be used for enhance the quality of an EMD encoded image.

Also all of these tecniques reveal interesting applications on the audio and music field as for example frame rate conversion or as digital audio effects.

We, in fact, will pursuit this aim and continue to explore the amazing world of fractals.

Appendix A

Algorithms for fractal encoding

Introduction

In charter 2 we saw the principles and concepts that lead to apply fractal theory to the image and video processing fields.

In this appendix we will see the implementation we made for a fractal encoder and decoder, based on the concepts we developed in the thesis.

We will discuss an algorithmic point of view instead of an actual implementation, like in C or Java, since it is more general and more intuitive.

The entire actual framework made for this study was entirely developed in ANSI C, and some parts of the algorithms we will discuss here will contain same of this code.

.

Bidimensional fractal encode

The two-dimensional fractal encoder works on gray-level images, or with one layer of color decomposition. To encode a color image, it should be decomposed in three color layer decomposition as separated RGB or YIQ layers.

Every image will be partitioned in squared domain and range blocks. We assume that:

- Range blocks have a constant size equal to R
- Domain blocks have a constant size equal to D, which is two times the size of a range block.
- The Domain Pool is a “Non Overlapped Domain Block”

The last restriction will be removed in a second evolution of the coder, in order to exploit the ORB and ORC method for zooming images.

Given a starting image μ_{orig} the encoder process will be:

for ever Range Block R_i on the partition obtained from the starting image μ_{orig} :

1) extract l’*i*-esim Range Block R_i ;

2) find the fractal transform of this block;

3) save the fractal code τ_i

end

The core of the fractal encoder is the second step, since the first and the last steps are simply memory access:

2.a) from the input Range Block R_i compute its luminance l_{R_i} and its contrast c_{R_i}

2.b) compute $|R_i|$ with the norm of the Range Block using the luminance and the contrast.

For every Domain Block D_j inside the Domain Pool:

2.c) subsample D_j to match Range Block's size

2.d) compute its luminance l_{D_i} and its contrast c_{D_i}

2.e) compute $|D_j|$ with the norm of D_j using l_{D_i} and c_{D_i}

For every isometry k from the isometry set:

2.f) compute the k-esim isometry $|D_j|_k$ starting from $|D_j|$

2.g) compute the error between $|R_i|$ and $|D_j|_k$

2.h) if the error is a local minimum, save τ_i composed by information on isometry and domain used.

end "isometry" loop

end "Domain Block" loop

Now we will take a closer look on each of these points:

2.a) The luminance l_{R_i} and the contrast c_{R_i} del of the range block R_i is computed the following way :

- Luminance l_{R_i} is the minimum value of luminance among all pixels that compose R_i :

$$l_{R_i} = \min_{\substack{1 \le x \le R \\ 1 \le y \le R}} \left[p_{R_i}(x, y) \right]$$

where $p_{R_i}(x, y)$ is a generic pixel of R_i whereas R is the size of the Range Block

- Contrast c_{R_i} is obtained by the overall sum of pixels inside the Range R_i. Before the addition, the previous luminance l_{R_i} is subtracted to every pixel's value.

$$c_{R_i} = \sum_{y=1}^{R}\sum_{x=1}^{R}\left[p_{R_i}(x,y) - l_{R_i}\right]$$

2.b) The normalization $|R_i|$ of the range block R_i is obtained:

1) From the pixels that belong to the Range Block R_i, the luminance l_{R_i} is subtracted (luminance shift)
2) Every pixel is then divided by the contrast c_{R_i} (contrast scaling)

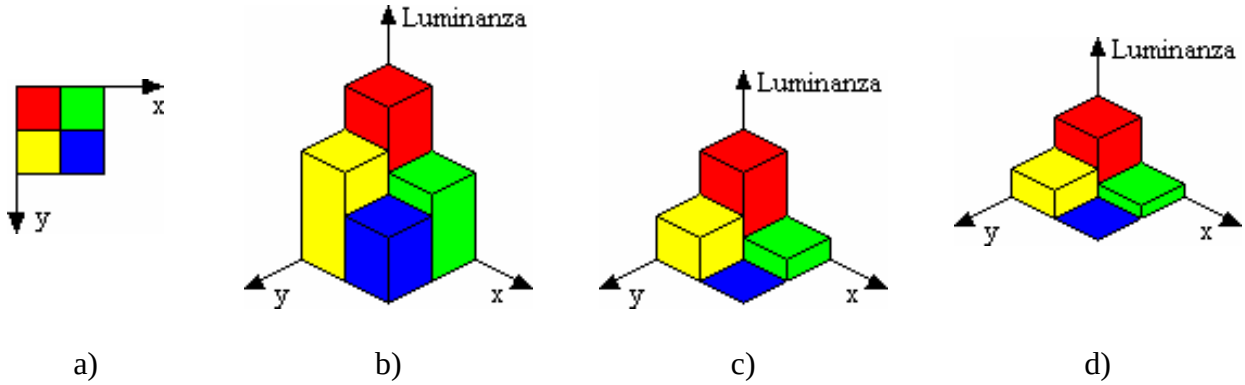

a) b) c) d)

Fig. 54: ***An example of normalization: a) the range block; b) a three-dimensional representation of the range block; c) luminance shift; d) contrast.***

We can explain the overall process using the given range block as an example.

10	7
5	4

It is easy to notice that $l_{R_i} = 4$. To obtain the contrast we subtract the luminance value to every pixel, and then we sum all the pixels together:

$$c_{R_i} = (10-4)+(7-4)+(5-4)+(4-4) = 10$$

2.c) The generic domain block D_j is subsampled by a factor of two (as we stated as a condition) to have the same dimension of the range block R_i

2.d) The same procedure of 2.a) is now executed on D_j

2.e) The same procedure of 2.b) is now executed on D_j

2.f) A k isometry is chosen

Identity	$\tau_1(\mu_{i,j}) = \mu_{i,j}$
Horizontal reflection	$\tau_2(\mu_{i,j}) = \mu_{i,n-j}$
Vertical reflection	$\tau_3(\mu_{i,j}) = \mu_{n-i,j}$
First diagonal reflection	$\tau_4(\mu_{i,j}) = \mu_{j,i}$
Second diagonal reflection	$\tau_5(\mu_{i,j}) = \mu_{n-j,n-i}$
90° counter-clockwise rotation	$\tau_6(\mu_{i,j}) = \mu_{n-j,i}$
180° counter-clockwise rotation	$\tau_7(\mu_{i,j}) = \mu_{n-i,n-j}$
270° counter-clockwise rotation	$\tau_8(\mu_{i,j}) = \mu_{j,n-i}$

Allowed isometries

2.g) To compare ranges and transformed domain we need a metric. As a first approximation we can use the simple MSE between pixels of $|R_i|$ and $|D_j|_k$:

$$MSE\left(|R_i|,|D_j|_k\right) = \frac{1}{R \cdot R}\sum_{y=1}^{R}\sum_{x=1}^{R}\left[p_{|R_i|}(x,y) - p_{|D_j|_k}(x,y)\right]^2$$

2.h) Finally the fractal code τ_i of the Range Block R_i is obtained considering:

- The coordinates (x_{D_j}, y_{D_j}) that identify the Domain Block D_j (founded as in 2.g that minimize the MSE error measure) on the encoding image.
- The isometry *k* that minimize the error measure.
- Luminance l_{R_i}, l_{D_j} and the contrast ratio:

$$c_i = \frac{c_{R_i}}{c_{D_i}}$$

All these steps are mandatory, to obtain an efficient matching between Range Blocks R_i and all the isometries of the subsampled Domain Block D_j. This can be proved with a simple example. Given the following Range Block and Domain Block (the Domain Block is already subsampled to match the Range Block size):

R_i

10	7
5	4

D_j

19	13
9	7

We can notice that they seem completely different from each other for every isometry applied to D_j.

The luminances of the blocks are: $l_{R_i} = 4$ and $l_{D_j} = 7$. As stated in 2.b.1 we can subtract the luminance to their respective blocks:

$R_i - l_{R_i}$

6	3
1	0

$l_{R_i} = 4$

$D_j - l_{D_j}$

12	6
2	0

$l_{D_j} = 7$

Now we can compute the contrast of the blocks and apply the ratio as in 2.h:

$$\frac{(R_i - l_{R_i})}{c_{R_i}} \qquad \frac{(D_j - l_{D_j})}{c_{D_j}}$$

0.6	0.3
0.1	0

$l_{R_i} = 4$

$c_{R_i} = 10$

0.6	0.3
0.1	0

$l_{D_j} = 7$

$c_{D_j} = 20$

As we can see now, the initials blocks that seemed different are now identical.

All the operations made are reversible.

Bidimensional Fractal Decoder

Once we have the fractal code τ computed with the method described above, we can reobtain a fractal approximation of its initial attractor (the initial image) μ_{orig}. We assume that:

- Range Blocks have a constant size of $R' = \beta \cdot R$
- Domain Blocks have a constant size D' which is two times the size of the Range Blocks
- The starting image of the decoding process μ_0 has a size that is β times the size of the initial encoded image μ_{orig}.

The factor β is the zooming factor used at the decoding stage to obtain variable different sizes of decode image.

Given the fractal code τ and a starting image μ_0 the decoding stage is composed by the following steps:

1) for m< α iterations

2) for every τ_i of τ

3) read from τ_i the domain block coordinates $\left(x_{D_j}, y_{D_j}\right)$

4) extract the Domain Block D_j situated at the position $\left(\beta \cdot x_{D_j}, \beta \cdot y_{D_j}\right)$ of μ_m

5) Compute a subsample approximation $D_j\Big|^{sub}$ of D_j to match the size of R_i

6) apply the *k* isometry extracted from τ_i to $D_j\Big|^{sub}$ obtaining $D_j\Big|_k^{sub}$

7) extract l_{R_i}, l_{D_j} and c_i from τ_i

8) apply luminance values and contrast to $D_j\Big|_k^{sub}$ obtaining $R_i\Big|_{decoded}$

9) write $R_i\Big|_{decoded}$ on μ_{m+1}

End τ_i loop

End iteration loop

The previous steps mean:

1) This loop cycles the whole decoding procedure α times: this is the cycle that generate the sequence of images that will converge toward the attractor (μ_{orig} or an expanded version of it)
2) This loop decode all the τ_i fractal transform related to the Range Block R_i
3) Reads from τ_i the coordinates $\left(x_{D_j}, y_{D_j}\right)$ of Domain Block D_j. This domain is the best transformed domain that the encoder found in the original image μ_{orig} for R_i
4) Since all the image is zoomed by a factor β, all the coordinates must be shifted of the same amount.

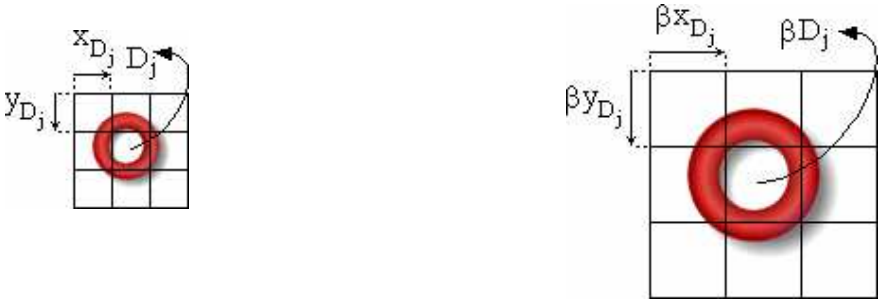

a) b)

Fig. 55: Shifting values of domain blocks for a zoomed replica of μ_{orig}

5) It is a simple subsampling operation that leads the size of D_j to match R_i's size
6) The isometry *k* that minimized the error during the encoding is applied to the domain block.
7) Read / write operations
8) The luminance l_{D_j} is subtracted to $D_j\big|_k^{sub}$ and all the pixels are then multiplied by the contrast factor c_i. After this step, we sum the luminance l_{R_i}. Now the range R_i is correctly reconstructed.
9) All the pixel of $R_i\big|_{decoded}$ are now copied into μ_0. The actual position of the block is obtained implicitly, since along the encoding the range blocks are ordered, for example by rows.

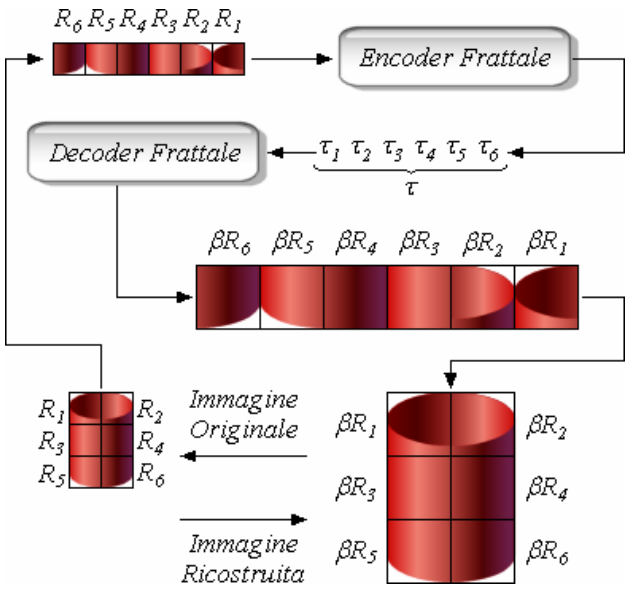

Fig. 56: Fractal decoding

As an example, given the following fractal code:

$$\tau_i = \left\{ x_{D_j} = 20; y_{D_j} = 4; k = 1; l_{R_i} = 4; l_{D_j} = 3; c_i = 0.5 \right\}$$

We extract from the decoding starting image μ_0 the Domain Block D_j at the position $\left(x_{D_j}, y_{D_j}\right)$. We can suppose that, after the subsampling operation the Domain Block is:

$$D_j\Big|^{sub}$$

19	13
9	7

We apply the isometry $k = 1$. From the table 1 we find that this is an identity, so $D_j\Big|^{sub}$ does not change. We now subtract from the Domain Block the luminance value l_{D_j}:

$$D_j\Big|_k^{sub} - l_{D_j}$$

16	10
6	4

And multiply by a contrast factor of c_i

$$\left(D_j\Big|_k^{sub} - l_{D_j}\right) \cdot c_i$$

8	5
3	2

Now we can add the luminance value l_{R_i} and obtaining the decoded Range block $R_i\big|_{decoded}$

$R_i\big|_{decoded}$

12	9
7	6

Now the Range Block is copied into μ_0 and the decoding process continues to the next Range Block.

Three-dimensional fractal CODEC

Basically the concept of a three-dimensional codec is the same of the bi-dimensional one. The difference is that now we have to work with three-dimensional blocks (or, better, cubes) , being the time axis the third dimension. Range and Domain blocks are now Cubes, and instead of an image we work with a sequence.

The concepts of luminance l_{R_i} and l_{D_j}, contrast c_{R_i}, c_{D_j} and their ratio c_i, do not change, but instead of being computed on blocks, they are computed on cubes.

Being in a three-dimensional space we need another offset coordinate for the domain block to be stored in the fractal code, and the set of isometries must be changed to include three dimensional affine transforms.

Bibliography

[1] R. H. Bartels, J. C. Beatty, and B. A. Barsky, "Hermite and Cubic Spline Interpolation." Ch. 3 in *An Introduction to Splines for Use in Computer Graphics and Geometric Modelling.* San Francisco, CA: Morgan Kaufmann, pp. 9-17, 1998.

[2] L.Polidori and J. Chorowicz, “Comparison of Bilinear and Brownian Interpolation for Digital Elevation Models,” USPRS Journal of Photogrammetry and Remote Sensing, No.48 pp. 18-23. 1993

[3] R.G. Keys, “Cubic Convolution Interpolation for Digital Image Processing,” IEEE trans on ASSP, No. 29, pag 11153-1160, 1981

[4] G.A. Thomas, “Distorting the time axis: motion compensated image processing in the studio,” IBC’88 IEE Conference Publication no 293, pp. 256-259.

[5] G.A. Thomas and H.Y.K. Lau, “Generation of high quality slow motion replay using motion compensation,” Conference Proceeding, IBC September 90, pp. 121-125.

[6] T. Chen, “Adaptive temporal interpolation using bidirectional motion estimation and compensation”, IEEE International Conference of Image Processing 2002, pp.313-316.

[7] K. Hilman, H.-W. Park, and Y.-M. Kim, “Using motion compensated frame-rate conversion for the correction of 3:2 pulldown artifacts in video sequences,” IEEE Trans. on CSVT, Vol. 10, No. 6, pp. 869-877, Sep. 2000.

[8] Al-Mualla, M.E.,“Motion field interpolation for frame rate conversion”, IEEE International Symposium on Circuits and Systems 2003, pp. II 652 -655.

[9] C.W. Tang, O.C. Au, “Comparison between block-based and pixelbased temporal interpolation for video coding”, IEEE Int. Sym. On Circuits & Systems, Vol. 4, pp.122-125, May 1998.

[10] B. Mandelbrot, “The Fractal geometry of nature”, Freeman & Co, S. Francisco, 1982.

[11] F. Hausdorff, “Dimension und äu ßeres ma ß”, Math. Ann. 79, 157-179, 1918.

[12] E. N. Lorentz, “The local structure of a chaotic attractor in four dimensions”, Physica 13D, 90-104, 1984.

[13] S. Barnsley and M.F. Demko, “Iterated function systems and the global construction of fractal,” Proc. Royal Soc. London, A399, pp. 243-275, 1985.

[14] A.E. Jaquin, “Image coding based on a fractal theory of iterated contractive image trasformation,” IEEE Trans. on Image Processing, vol. 1, no. 1, pp. 18-30, Jan. 1992.

[15] Y. Fisher, and R. D. Boss, and E. W. Jacobs, “Fractal image compression: image and text compression”, Kluwer Academic Publishers, Norwell MA, 1992.

[16] M. Polvere, and M. Nappi, “Speed-Up in Fractal Image Coding: Comparison of Methods,” IEEE Trans. on Image Processing, vol. 9, no. 6, pp. 1002-1009, Sept. 2000.

[17] S. Mallat, “A theory for multiresolution signal decomposition: The wavelet representation,” IEEE Trans. Pattern Analysis and Machine Intelligence,1989, vol. 11, pp. 674-693.

[18] E Reusens, “Overlapped Adaptive Partitioning for Image Coding Based on Theory of Iterated Function Systems,” Proc. IEEE ICASSP, vol 5, pp 569-572, Adelaide, Australia, 1994.

[19] K.U. Barthel and T. Voye, “Three-Dimensional Fractal Video Coding,” Proc. IEEE ICIP-95, vol 3, pp. 260-263, Washington, D.C., 1995.

[20] K.U. Barthel, T. Voye and G. Ruhl “Combining Wavelet and Fractal Coding for 3-D Video Coding,” Proc. IEEE ICIP-96, vol. I, pp 181-185, Lausanne, 1996.

[21] M. Ancis and D.D. Giusto, “Image data compression by adaptive vector quantization of classified wavelet coefficients,” Proc. IEEE PACRIM Conference, pp. 330-333, Victoria, Canada, 1997.

[22] S. Wolf, “Measuring the End–to–End Performance of Digital Video Systems”, IEEE Trans. on Broadcasting, vol. 43, no. 3, pp. 320–328, Sept. 1997

[23] ITU-R Recommendation BT.1683, “Objective perceptual video quality measurement techniques for standard definition digital broadcast television in the presence of a full reference”, International Telecommunication Union, Geneva, Switzerland, 2004.

[24] Video Quality Research project, http://www.its.bldrdoc.gov/n3/video/Default.htm.

[25] E. Polidori, J.-L. Dugelay, “Zooming using Iterated Function Systems,” NATO ASI Conference on Fractal Image Encoding and Analysis, Trondheim, July 1995.

[26] D. D. Giusto, M Murroni and G. Soro “Slow Motion Replay of Video Sequences using Fractal Zooming,” *IEEE Trans. on Consumer Electronics*, vol. 51, Issue 1,pp.103−111, February 2005.

[27] B. Hurtgen, P. Mols. and S.F. Simon, “Fractal transformation coding of color images,” Visual *Comunication and Image Processing, SPIE Proceeding*, 1994.

[28] Y. Zhang and L.M. Po. “Fractal color image compression using vector distortion measure,” *International Conference on Image Processing.* vol. 3, October 1995.

[29] I. M. Danciu and J. C. Hart, “Fractal color compression in the L*a*b* uniform color space,” Data Compression Conference, March 1998.

[30] Y. Rubner, L. J. Guibas and C. Tomasi, “The earth mover’s distance as a metric for image retrivial”, Technical Report STAN-CS-TN-98-86, Stanford Computer Science Department, Sept. 1998.

[31] Recommendation ITU-R BT.709-5, “Parameter values for the HDTV standards for production and international programme exchange” ,1990, 1994,1995, 1998, 2000, 2002.

[32] J. B. MacQueen: "Some Methods for classification and Analysis of Multivariate Observations, *Proceedings of 5-th Berkeley Symposium on Mathematical Statistics and Probability"*, Berkeley, University of California Press, 1:281-297, 1967

[33] S. Cohen and L. Guibasm, “The Earth Mover's Distance under transformation sets,” *International Conference on Computer Vision.* Vol. 2, pp. 1076 – 1083, Sept. 1999.

[34] S. T. Rachev. “The Monge-Kantorovich mass transference problem and its stochastic applications,”. Theory of Probability and its Applications, XXIX(4), pp. 647−676, 1984.